Scattering Centre Extraction in High Resolution Radar Imaging

Prepared by:

R.F. van Schalkwyk

VSCRIC005

Supervised by:

Prof. M. Inggs

Department of Electrical Engineering

February 2014

A dissertation submitted to the Department of Electrical Engineering,

University of Cape Town,

in partial fulfilment of the requirements

for the degree of

Master of Engineering specialising in *Radar and Electronic Defence*.

Declaration

1. I know that plagiarism is wrong. Plagiarism is to use another's work and pretend that it is one's own.
2. I have used the IEEE convention for citation and referencing. Each contribution to, and quotation in, this project report from the work(s) of other people, has been attributed and has been cited and referenced.
3. This project report is my own work.
4. I have not allowed, and will not allow, anyone to copy my work with the intention of passing it off as their own work or part thereof.

Signature of Author .....

Pretoria
13 February 2014

Abstract

The objective of this dissertation is to establish a preferred approach to decomposing electromagnetic scattered field data into a sparse representation of scattering centres. In order to complete the research objective, a performance comparison between two scattering centre extraction techniques is presented. The selected techniques were chosen, as preferred candidates, from two distinct classes of algorithms. The first technique was chosen from a class of deconvolution-based algorithms and the second from a class of super-resolution techniques.

The performance comparison places emphasis on applications in controlled environments such as high fidelity electromagnetic simulations which allow for the generation of high-quality high signal-to-noise ratio data. The study makes use of synthetic scattered field data generated in Matlab and FEKO (a computational electromagnetic software package) and evaluates the performance of the techniques in terms of: resolution, measurement precision and radar cross section re-synthesis. The results from the evaluation have shown that under low signal-to-noise ratio conditions, the deconvolution technique performs better; while under high signal-to-noise conditions, the super-resolution technique is shown to perform better.

A performance-limiting characteristic, in the use of conventional polar reformatting in the super-resolution technique, was identified during the study. This led to the development of an iterative polar reformatting technique which makes direct use of estimated scattering centers. Initial results have shown that the new approach offers significant performance improvement and highlighted that attributes from both classes add value in the preferred approach.

Acknowledgements

I would like to thank ARMSCOR for funding the larger part of this research effort, in line with work in the field of Radar Cross Section (RCS) modelling. CSIR for both time to work on the study, as well as the use of their resources. Johan Smit for his guidance throughout the study as well as his assistance in both preparing and reviewing this minor dissertation document, as well as Prof. Michael Inggs for his guidance and assistance in reviewing this minor dissertation document. I would also like to thank some of my work colleagues, namely Jacques Cilliers, Chris Mocke and Willie Nel for many insightful conversations which helped steer the direction of the work.

Terms of Reference

The focal point of the study is the decomposition of high resolution radar images into sparse representations using point scatterers as the basis functions. The planned scope covers:

1. A literature survey which aims to identify techniques used in point scatterer extraction as well as known limitations.

2. An analysis of at least two of the techniques presented in literature. The planned simulation work covers:

· Analysis using ideal point scatterers.

· Analysis using a few objects, that exhibit localised scattering characteristics, simulated using a computational electromagnetic software package (FEKO).

3. A performance comparison between the selected techniques using the following metrics: resolution, measurement precision (through Monte Carlo analysis) and RCS re-synthesis.

4. The findings and results are to be presented as well as any contribution I have made during the study.

5. My interpretation of the results, limitations and trends as well as scope for future work.

Contents

List of Figures

List of Tables

List of Symbols

ϕ_n	—	Aspect angle
f_m	—	Carrier frequency (instantaneous)
f_c	—	Effective carrier frequency (over full agile bandwidth)
P	—	Number of scattering centers
BW	—	Total agile bandwidth
Ω	—	Total image rotation angle
c	—	Speed of light
E_s	—	Electromagnetic scattered field
E_i	—	Electromagnetic incident field
R	—	Radar range
Y_{max}	—	Unambiguous cross range
X_{max}	—	Unambiguous slant range
$\mathbf{Y}$	—	Data matrix
$\mathbf{R}$	—	Covariance matrix
$\mathbf{U}$	—	Eigenvector matrix of $\mathbf{R}$
$\mathbf{\Psi}$	—	Rotation operator matrix estimate
$\mathbf{\Phi}$	—	Rotation operator matrix
$\mathbf{T}$	—	Eigenvector matrix of $\mathbf{\Phi}$
λ_i	—	i^{th} eigenvalue of $\mathbf{R}$
VV	—	Vertical polarization on transmit and receive

Nomenclature

AIC — Akaike Information Criterion.

CEM — Computational Electromagnetics.

CLEAN — A class of deconvolution-based algorithms.

Cross Range — An imaging axis perpendicular to the direction of the EM propagation.

Deconvolution — A technique used to reverse the process of convolution such as the removal of the system response from a signal.

EM — Electromagnetic.

EP — Evolutionary Programming.

ESPRIT — EStimation of Signal Parameters via Rotational Invariance Techniques. From a class of parametric spectral estimation techniques which make use of the underlying properties of the covariance matrix.

FFT — Fast Fourier Transform.

ISAR — Inverse Synthetic Aperture Radar. A high-resolution radar imaging technique making use of frequency diversity to improve slant range resolution and angular diversity to improve cross range resolution. Angular diversity is achieved in this technique through the target's rotational motion relative to the Radar.

MDL — Minimum Description Length.

Monostatic — A co-located transceiver configuration.

MUSIC — MUltiple SIgnal Classification. From a class of parametric spectral estimation techniques which make use of the underlying properties of the covariance matrix.

PFT — Polynomial Fourier Transform.

Polar Reformatting — A technique used to transform measurements made in the polar space to Cartesian space.

RCS — Radar Cross Section.

RMSE — Root Mean Square Error.

SAR — Synthetic Aperture Radar. A high-resolution radar imaging technique making use of frequency diversity to improve slant range resolution and angular diversity to improve cross range resolution. Angular diversity is achieved in this technique through the radar's rotational motion relative to the imaging scene or target.

Scattering Center/ Point Scatterer — Localised re-radiation from an object that can be approximated as an ideal point source.

Slant Range — An imaging axis parallel to the direction of the EM propagation where the axis origin is the centre of rotation of the scene or target.

SNR — Signal to Noise Ratio.

SVD — Singular Value Decomposition.

Chapter 1

Introduction

1.1 Background to the study

Decomposing high resolution radar images into sparse representations is an active field of research in both compressed sensing and target classification. In high resolution radar imagery, each image is formed through the complex combination of electromagnetic back-scatter from many different scattering mechanisms within each scene. The image can thus be represented by a combination of components (defined as bases) that each map to specific scattering mechanisms with physical relevance. One such basis, used in high resolution radar imagery, is that of the ideal point scatterer (i.e. scattering centre). In the use of this basis it is assumed that the electromagnetic back-scatter from an object can be well approximated by the combined effect of a finite number of localised (i.e. point like) scattering sources. The literature shows that certain man-made objects map well to this model with structures comprising multiple corner reflectors, cavities and edges.

Decomposing an image into its bases, irrespective on the choice of basis model chosen, can then be seen as an estimation problem where the parameters of each basis are estimated, that best describe the data. When the point scatterer basis is chosen and under specific constraints, the objective simplifies to one of a spectral estimation problem. Estimating the location and amplitude of point sources

by conventional Fourier analysis has led to the development of many variants in the CLEAN class of algorithms. Compared to direct Fourier analysis, these techniques have been shown to offer improved dynamic range. This allows for resolving weaker scattering centres that are hidden below the sidelobes of the stronger scattering components. The use of parametric spectral estimation techniques, dubbed super-resolution techniques, have also been proposed and have been reported to offer improved resolution and measurement precision compared to direct Fourier analysis.

Given advancements in both 3D scanning technologies and Computational Electromagnetics (CEM) high fidelity simulations of the expected scattered field data from electrically large objects are now possible. This allows for the generation of synthetic, high precision, high resolution radar imaging data. Using synthetic data for image decomposition should theoretically yield higher precision estimates of the basis parameters compared to measured data which is corrupted by measurement noise.

1.2 Scope and Limitations

In order to realise high precision image decomposition, this study evaluates two known scattering centre extraction techniques in terms of their performance in controlled environments. Control implies that significant parameters, such as frequency and target orientations a function of time, are controlled and hence known.

The performance metrics considered in the study include: resolution, measurement precision (through Monte Carlo analysis) and Radar Cross Section (RCS) re-synthesis. The evaluation makes use of simulated synthetic scattered field data generated in both Matlab and a CEM software package (FEKO).

As a result of the limited scope required for a minor dissertation, emphasis was placed on emerging properties of the performance comparison for a limited number of scenarios. This is in contrast to establishing a comprehensive global

performance value valid over all imaging parameters and scenes.

The following assumptions are made in the study:

1. The observation point (monostatic configuration) is situated in the far-field such that the plane-wave assumption is valid.
2. The amplitude and location of each scattering centre, over a set of frequency and angular diverse measurements, is assumed constant, provided that the bandwidth is narrow and rotation angle small.
3. Imaging is constrained to two dimensions (slant and cross range).
4. Only conventional polar reformatting techniques, as found in the high resolution radar imaging textbooks, are considered.

1.3 Overview

The structure of this minor dissertation is organized as follows: Chapter 2 presents a literature review on two classes of scattering centre extraction techniques. The first is a class of deconvolution-based algorithms called CLEAN and the second a class of super-resolution techniques. The review demonstrates the maturity of the field through highlighting many extensions and advancements made over the passed several decades.

The inherent link between the ideal point scatterer model and high resolution radar imaging is briefly addressed in Chapter 3. The algorithms for 2D EP-based CLEAN and 2D ESPRIT are also presented together with the performance metrics used to evaluate them.

Chapter 4 presents an analysis on the influence polar reformatting has on super-resolution techniques. As is shown, conventional interpolation-based approaches do not decouple frequency from angle perfectly. When applying spatial smoothing this limitation leads to the introduction of partially correlated spectral com-

ponents as well as processing noise. This attribute can be demonstrated by an analysis of the eigenvalues of the covariance matrix as shown in Figure 1.1.

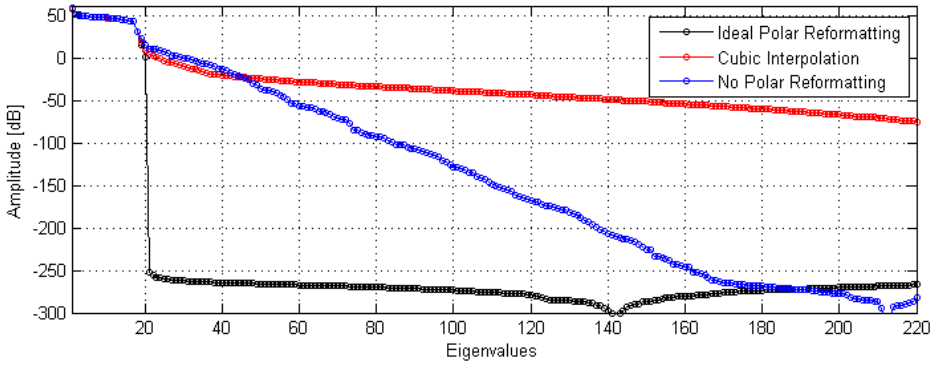

Figure 1.1: Influence of polar reformatting on ESPRIT from Chapter 4.

In addition, Chapter 4 presents a iterative polar reformatting technique developed during the study. This technique was developed based on the assumption that the scattering centre estimates could be used to directly decouple frequency and angle through the ideal point scatterer model.

Several research questions are defined in Chapter 5. In addition, the procedures and experimental configurations used to address these questions are also presented. Matlab was used to generate synthetic data based on the ideal point scatterer model while more representative synthetic scattered field data was generated using FEKO. The primary geometry considered in the study is shown in Figure 1.2.

The results are presented in Chapter 6. A performance comparison between EP-based CLEAN and ESPRIT for synthetic scattered field generated in both Matlab and FEKO is presented. In addition, the performance gains using the new iterative polar reformatting approach are demonstrated. These gains are evident by a reduction in the location RMSE as well as an improvement in the quality of RCS re-synthesis, as highlighted in Figure 1.3.

Chapter 7 concludes the study with a discussion of the results, highlighting important trends and findings, followed by possible extensions to the work.

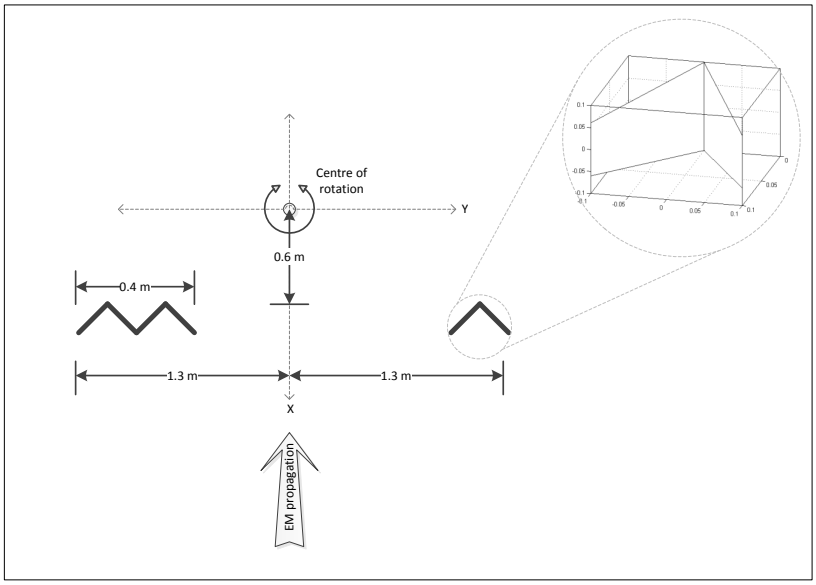

Figure 1.2: Simulation geometry from Chapter 5.

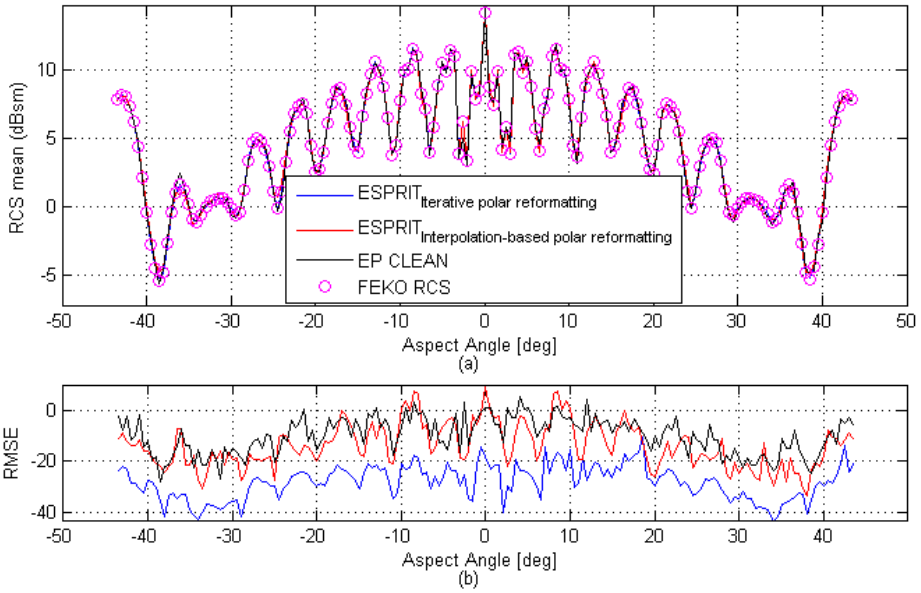

Figure 1.3: Re-synthesised RCS as a function of aspect angle from Chapter 6.

Chapter 2

Literature Review

2.1 Introduction

When an object is illuminated by an electromagnetic (EM) wave a portion of the energy is absorbed and the remainder re-radiated. This re-radiation is influenced by both the properties of the EM wave (such as wavelength) and specific object attributes such as: type of material, geometry and structure of the surface. Through a complex combination of specular (mirror-like) reflections and diffuse scattering from edges and discontinuities along the surface, some of the regions on the object provide localized re-radiation of the energy towards an observation point. These localized regions are often referred to as *scattering centres* or *point scatterers*. Given the nature of the re-radiating source, these scattering centres provide a physically relevant and concise description of an object. The use of a scattering centre model thus provides a way to represent an object as a sparse collection of attributed scattering centres. As highlighted in [1, 2] some advantages of this representation include:

1. RCS data or SAR/ ISAR imagery compression where re-synthesis can be achieved quickly.

2. Extrapolation and interpolation of scattered field data.

3. High resolution analysis of EM scattering with applications in:
   (a) Feature extraction for Automatic Target Recognition (ATR),
   (b) RCS reduction in stealth design and
   (c) Elimination of spurious scattering in compact ranges.

With clear application in high resolution radar imagery, a number of scattering centre extraction techniques have been developed over the past four decades and appear to assign well to two classes, namely:

1. A class of deconvolution-based techniques called CLEAN, and
2. A class of supper-resolution techniques based on the eigenstructure of the covariance matrix

An overview of the two approaches is presented in the following sections.

2.2 CLEAN Class of Algorithms

The first technique attributed to the CLEAN class of algorithms was initially developed in radio astronomy for non-coherent radiation fields derived from independently radiated point sources such as stars. Tsao and Steinberg [3] were first to extend the technique to coherent radiation fields for application in radar imaging. The coherent CLEAN technique attempts to recover weaker signals that are usually masked by the high sidelobes of stronger signals. This is achieved through an iterative process of identifying the strongest signal and removing the estimated system response corresponding to its contribution. The process is then terminated once a specific threshold is reached. The CLEAN technique was first applied to ISAR imagery by Yiping and Pingping [4]. In their contribution, the Fast Fourier Transform (FFT) was used to estimate the scene and the process terminated using a threshold based on a single reference range bin.

The operation of CLEAN requires the assumption of isolated independent sources to hold. An extension to address distributed targets, often found in high resolution radar imagery, called Sequence CLEAN was proposed by Steinberg *et al.* [5]. In their approach, a sequence of the n^{th} largest peaks is selected that minimises the energy in contrast to always selecting the largest peak at each iteration. While this initial effort saw every possible sequence tested, which was computationally expensive, an extension by Bose [6] called Breeder Genetic Algorithm (BGA) assisted Sequence CLEAN was proposed to address this limitation. Utilizing the heuristic nature of evolutionary computation, the convergence time to resolve the optimal sequence was reduced. A second advantage of this approach was that the search space (number of peaks selected at any time) could be increased without increasing the computational load.

A CLEAN technique making use of Evolutionary Programming (EP) called EP-based CLEAN was proposed by Choi and Kim [7]. In their approach the parameters of the ideal point sources are estimated on each iteration by minimisation of a cost function. The cost function makes use of the ideal point scatterer model where the estimated parameters converge through a process of natural selection. This extension was shown to offer a small improvement in resolution compared to its FFT counterparts with a distinct advantage that the data does not require any polar reformatting.

An extension of the CLEAN technique for improved application in ISAR imagery saw the introduction of a modified CLEAN technique by Yang *et al.* [8]. In this approach, the polynomial Fourier transform (PFT) is used for cross range analysis of range compressed data as apposed to the use of conventional FFT based solutions. This was done in order to address non constant Doppler components often encountered in ISAR imagery. The primary ideal behind the modified approach is an iterative estimation of the scatterers' Doppler and chirp rates where scatterer detection is energy-threshold based. An extension to their approach was later presented by Martorella *et al.* [9] called Statistical CLEAN (S-CLEAN). In S-CLEAN, a Gaussianity test is applied to each cell in order to detect scatterers. This approach is shown to offer improved performance compared to the more heuristic detection process of Yang *et al.* [8]. In addition, the statistical detector

of [9] is directly related to the false alarm rate.

2.3 Super-resolution Techniques

The Pisarenko harmonic decomposition, proposed by Pisarenko [10], was the first frequency estimation method that was based on the eigendecomposition of the covariance matrix and its partitioning into two orthogonal subspaces. The first subspace is called the signal subspace given a direct relationship to the vector space spanned by the pure signal components. The second subspace is called the noise subspace. The work from Pisarenko [10] led to the development of many closely related super-resolution techniques.

In order to draw a distinction between the approaches, the techniques are split into two sub-classes:

1. Super-resolution techniques based on an orthogonality between the estimated signal and noise subspaces. These techniques make use of the estimated noise subspace to resolve the spectral components.
2. Super-resolution techniques based on a rotational invariance of the signal subspace as a function of translational invariance between two matched sensor arrays or overlapping subarrays of uniformly sampled data. These techniques make use of the estimated signal subspace to resolve the spectral components.

From the first sub-class, the approach of [10] proved to be too sensitive as a result of only using one basis from the noise subspace. Schmidt [11] extended this approach to a more robust form called MUltiple SIgnal Classification (MUSIC). In MUSIC, multiple bases from the noise subspace are used to project onto a set of mode vectors resulting in an averaged *pseudo-spectrum* where the peaks of this spectrum are indicative of the signals that span the signal subspace. Given that the pseudospectrum is formed through dividing by the projection, the amplitudes of the peaks are a function of orthogonality and not power.

Shortly after the introduction of MUSIC, Estimation of Signal Parameters via Rotational Invariance Techniques (ESPRIT) was proposed by Kailath *et al.* [12]. In contrast to MUSIC, their approach makes direct use of the signal subspace to estimate the spectral components and offers several advantages over MUSIC including improved performance, reduced computational load and reduced sensitivity to array perturbations. In its simplest form, spectral estimation is achieved through solving a set of coupled one-dimensional generalized eigenvalue problems for a set of matrix pairs. These matrix pairs are formed from different overlapping subsets of the signal subspace and are chosen such that the rank reducing numbers (generalized eigenvalues) are directly related to the spectral components.

Over the ensuing years many of the limitations plaguing the initial approaches were addressed. Max and Kailath [13] were first to produce a more robust model based estimator using both the Akaike Information Criterion (AIC) and Minimum Description Length (MDL) criterion. The number of signals, required in order to split the signal and noise subspace, was obtainable merely by minimizing the AIC or MDL criterion. This was in contrast to initial efforts using thresholds and hypothesis testing. The requirement of uncorrelated or partially correlated sources was also addressed by Kailath *et al.* [14] through the proposal of a one-dimensional spatial smoothing technique. ESPRIT was also later extended to a Total Least Squares (TLS) implementation called TLS-ESPRIT by Roy and Kailath [15].

Odendaal *et al.* [16] were first to extend MUSIC to two dimensional high resolution radar imagery. Their contribution included an extension of the spatial smoothing technique to two dimensions with results that showed improved resolution compared to conventional Fourier analysis. While some previous work in two dimensional spatial smoothing had been done by Chen *et al.* [17] prior to [16], an extension to decorrelate multiple signals was only formally treated after the fact by Chen in [18]. Subsequently both MUSIC and ESPRIT, also with emphasis in high resolution radar imagery, were extended to three dimensions by Dobre and Radoi [19] and to multiple dimensions by Radoi *et al.* in [20].

It is important to note that just prior to the work presented by Odendaal [16], a few eigendecomposition techniques emerged that make use of singular value decomposition (SVD) of the data matrix. While treated in much of the literature as novel approaches, the author believes that they should be classed under the banner of ESPRIT, given the plural *Techniques* in the definition of ESPRIT and the fact that these techniques make direct use of the same rotational invariance attribute of the signal subspace. One such approach is the Matrix Enhancement and Matrix Pencil (MEMP) method of Hau [21]. In MEMP, the data matrix is re-arranged into a enhanced matrix of block Hankel structure followed by SVD and the realization of one-dimensional coupled eigenvalue problems. With direct relationships between covariance matrix eigendecomposition and SVD as well as the block Hankel structure and the two dimensional spatial smoothing technique from Odendaal [16]. It is quickly seen that these approaches make use of the same underlying algebra with only slight differences between techniques, such as the methods used to couple the generalized eigenvalues into correct pairs. However, these approaches have shown to add value by drawing attention to the correct underlying model of the two dimensional spatial smoothing technique where extension through multiple dimensions is now fairly intuitive. This attribute is demonstrated by the fact that an increase in dimension translates directly to solving an addition one-dimensional generalized eigenvalue problem, followed by correct pairing with lower dimensions.

2.4 Conclusion

The techniques used in scattering centre extraction, with emphasis on high resolution radar imagery, have undergone a fair amount of refinement over the past three decades. From the literature, the usefulness of the CLEAN class of algorithms has been demonstrated in both simulations [6, 7], as well as on measurements from targets in the field [4, 9]. While demonstrating a good robustness to noise, these techniques are shown to be limited in resolution and, as a result, offer reduced performance over distributed targets.

The parametric spectral estimation techniques have also undergone a fair amount of refinement through extension for application in high resolution radar imagery. The usefulness and performance of these techniques has been shown through several sets of results presented in the literature. With experiments ranging from simulations comprising ideal point scatterers and computational electromagnetics [22, 23] to measurements of model aircraft [16, 24] and an aluminum cone [25] in anechoic chambers.

While the results from the super resolution techniques offer improved performance compared to direct Fourier analysis as shown by Burrows [25], most of the performance comparisons are confined to within specific classes. While Choi and Kim [7] present a comparison between their EP-based CLEAN and MEMP their results place emphasis on low SNR application and do not address any emerging properties influencing biases in the results.

As a result of this gap in the literature, this study aims to provide a performance comparison between the prominent super-resolution technique (ESPRIT) and a model based deconvolution based technique (EP-based CLEAN) with emphasis placed on controlled environments with high SNR.

Chapter 3

Theoretical Background

The following section provides an overview of the models, mathematical techniques and algorithms underpinning the work presented in this study. The objective of this overview is to present and link the mathematical concepts; it is not an in-depth treatment of each principle as found in relevant literature.

An outline of the work presented is summarized in Figure 3.1

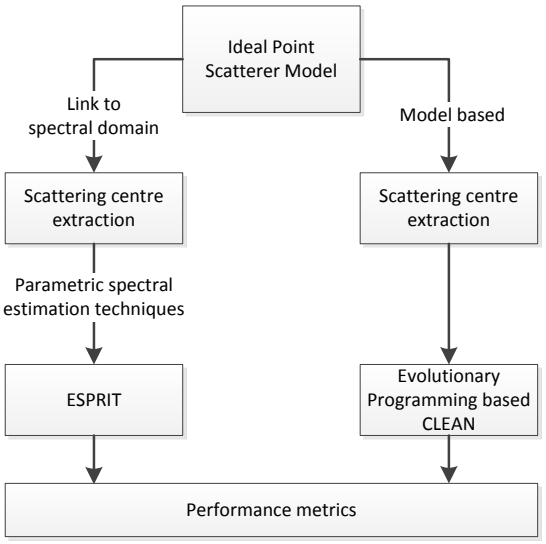

Figure 3.1: Theoretical background overview.

3.1 Ideal Point Scatterer Model

When the assumption is made that the EM scattered field re-radiating from an object originates from a finite number of localised scattering mechanisms. The EM scattered field, in the absence of noise, is well approximated as the sum of the contributions from all point sources, as shown in Caner [1] through

$$E^s(m,n) = \sum_{i=1}^{P} a_i \exp(-j\frac{4\pi f_m}{c}(\cos(\phi_n)x_i)) \exp(-j\frac{4\pi f_m}{c}(\sin(\phi_n)y_i)) \qquad (3.1)$$

The radar centre frequency is defined by f_m and the angle relative to the observation point by ϕ_n. The propagation velocity of the EM wave is assumed to equal the speed of light c for P scattering centres with amplitudes a_i and locations x_i and y_i in Cartesian space.

3.2 Image Estimation

When the target's location and orientation is known relative to an observation source at any point in time (defined as controlled environment in this study) the amplitude and location of each scattering centre can be estimated directly through Equation 3.1.

When the total look-angle is small ($< 5^o$) and the bandwidth narrow ($<< 0.1f_c$), Equation 3.1 can be approximated by

$$E^s(m,n) = \sum_{i=1}^{P} a_i \exp(-j\frac{4\pi f_m}{c}x_i) \exp(-j\frac{4\pi f_c}{c}\phi_n y_i) \qquad (3.2)$$

as a result of

$$\begin{aligned} \cos(\phi_n) &\cong 1 \\ \sin(\phi_n) &\cong \phi_n \end{aligned} \tag{3.3}$$

and

$$f_m \cong f_c \tag{3.4}$$

where f_c represents the carrier frequency at the centre of the agile bandwidth.

Given frequency diversity in the primary dimension and angular diversity in the secondary dimension the estimation problem is simplified, as Equation 3.2 maps directly through any 2D spectral estimation technique into a 2D image. The locations and amplitudes of the scattering centres are resolved by estimating the corresponding spectral components.

This 2D image is defined in terms of a slant range (direction parallel to the propagation of the EM wave) and cross range (direction perpendicular to the the slant range). Slant range attributes are a function of frequency diversity and cross range attributes a function of angular diversity.

This approach forms the underlying principles for the high resolution radar imaging techniques known as Synthetic Aperture Radar (SAR) and Inverse Synthetic Aperture Radar (ISAR). SAR obtains angular diverse measurements of a target based on the rotational motion of its own platform, whereas ISAR obtains angular diverse measurements of a target based on the target's rotational motion relative to the radar.

The conventional Fourier relationship between measurement parameters and corresponding image parameters as defined in Caner [1] is summarised in Table 3.1.

Table 3.1: High resolution radar imaging parameters

Image domain	Measurement domain
Δx	$\frac{c}{2BW}$
Δy	$\frac{c}{2f_c\Omega}$
X_{max}	$\frac{N_x c}{2BW}$
Y_{max}	$\frac{N_y c}{2f_c\Omega}$

The total agile bandwidth BW and image rotation angle Ω defines the achievable image sample resolutions in slant and cross range respectively. The unambiguous slant range X_{max} is a function of the number frequency steps N_x and the unambiguous cross range Y_{max} a function of the number of discrete samples in angle N_y.

When the assumption of small-angle and narrow band-width is removed the scattered field data requires reformatting in order to make use of the same spectral estimation techniques. This reformatting is done by interpolating the original data to a uniform Cartesian grid through the relationships

$$\begin{aligned} f_m^x &= f_m \cos(\phi_n) \\ f_n^y &= f_m \sin(\phi_n) \end{aligned} \tag{3.5}$$

where the form of the interpolated data better matches a 2D spectral estimation problem.

$$E^s(m,n) = \sum_{i=1}^{P} a_i'' \exp(-j\frac{4\pi f_m^x}{c} x_i'') \exp(-j\frac{4\pi f_n^y}{c} y_i'') + n_c(m,n) \tag{3.6}$$

As a result of polar reformatting, a'', x'' and y'' are corrupted versions of a, x and y along with the introduction of a complex noise component $n_c(m,n)$.

3.3 Scattering Centre Extraction Techniques

As shown in Section 3.2, the scattering centre extraction problem is treated in its simplest form as an estimation of the parameters in Equation 3.1. This requires an estimation of the number of scattering centres as well as their locations and amplitudes. The algorithms of two model based scattering centre extraction techniques are presented next.

3.3.1 2D EP-based CLEAN

Two dimensional EP-based CLEAN makes direct use of Equation 3.1 through a cost function defined by

$$J_p = \sum_{m=1}^{M} \sum_{n=1}^{N} \left| E_p(m,n) - a_p \exp\left(-j\tfrac{4\pi f_m}{c}(\cos(\phi_n)x_p + \sin(\phi_n)y_p)\right)\right|^2 \tag{3.7}$$

where the algorithm converges for the parameter set (amplitude a_p and locations x_p and y_p) that minimize the cost for P scattering centres iteratively.

Fourier variants of CLEAN make use of either the FFT of PFT to estimate the scene and therefore requiring polar reformatting. In contrast, EP-based

CLEAN performs processing directly on the scattered field data thereby avoiding processing artifacts introduced through the polar reformatting step.

The 2D EP-based CLEAN algorithm from Choi and Kim [7] is presented as follows:

1. Initialisation:
   Initialise iteration index: $p = 1$ and residual scattered field: $E_p(m,n) = E(m,n)$

2. Parameter extraction through EP subroutine:
   Obtain coefficients (a_p, x_p and y_p) that minimise the cost function of Equation 3.7 through the following subroutine:

   (a) Initialise:
   Initialise generation index $k = 1$ and generate N_p trial solutions from a uniform distribution within the given image limits: $\boldsymbol{a} = (a_1, a_2, ...a_{N_p})$, $\boldsymbol{x} = (x_1, x_2, ...x_{N_p})$ and $\boldsymbol{y} = (y_1, y_2, ...y_{N_p})$.

   (b) Evaluate:
   Evaluate the cost $J_p(a_i, x_i, y_i)$ for each parent solution.

   (c) Mutation:
   For each of the N_p parents a_i, x_i and y_i generate offspring $a_i^{'}, x_i^{'}$ and $y_i^{'}$ as follows

$$\begin{aligned} h_i^{'} &= h_i + \sigma_i^h N_i^h(0,1), \\ \sigma_i^{'h} &= \sigma_i^h \exp(\tau^{'} N(0,1) + \tau N_i^h(0,1)) \end{aligned} \tag{3.8}$$

   where h defines the parameters a, x or y and σ_i^h the corresponding standard deviation. $N_i^h(0,1)$ is a normally distributed random number with $\tau^{'}$ and τ as user defined parameters. These two parameters are used to constrain the rate at which the variance is reduced and thus directly related to population size and required convergence speed.

   (d) Evaluation:
   Evaluate the cost $J_p(a_i^{'}, x_i^{'}, y_i^{'})$ for each offspring solution.

(e) Selection:
Select N_p solutions out of the $2N_p$ solutions having the most wins. The most wins is defined as the N_p solutions with the smallest cost values.
Increase generation index: $k = k + 1$

(f) Termination check:
Proceed to step (c) or terminate if convergence criteria has been met.

3. Cancellation:
Subtract the estimated scattered field contribution as a result of parameter estimates (a_p, x_p and y_p)

$$E_{p+1}(m,n) = E_p(m,n) - a_p \exp\left(-j\tfrac{4\pi f_m}{c}(\cos(\phi_n)x_p + \sin(\phi_n)y_p)\right), \quad m = 1, ..., M \quad and \quad n = 1, ..., N. \tag{3.9}$$

4. Termination check:
Return to Step 2 or terminate if convergence criteria has been met, or desired number of scattering centres has been extracted.

While the EP-based CLEAN algorithm is not prescriptive regarding termination criteria the decision on when to terminate is influenced by the fact that after each iteration the scene comprises the following three components:

1. Scattering centres not yet found,
2. Residual components from imperfect cancellation of previously estimated scattering centres and
3. Random components from noise.

This characteristic implies that setting an amplitude threshold solely based on the noise floor will result in estimates from residual components being detected as scatterers. In contrast, setting a threshold which limits residual detections not

only requires a complex evaluation as to how well each component was canceled but will also reduce the sensitivity of the algorithm to smaller targets.

3.3.2 2D ESPRIT

ESPRIT, like other subspace eigenanalysis based algorithms, exploits the underlying properties of the autocorrelation matrix eigenstructure, which is equivalent to the autocovaraince matrix if zero mean complex sinusoids is assumed. Given that the autocorrelation matrix is Hermitian symmetric, the eigendecomposition produces real eigenvalues and orthogonal eigenvectors. The multidimensional vector space that contains the observations can thus be split into two orthogonal subspaces called the signal subspace and noise subspace respectively. Since the vectors (comprising the spectral components) that form the signal span the same signal space, as shown in Caner [26], there exists some transformation matrix $\boldsymbol{T}$ that relates the orthonormal bases to the original vectors. This transform then allows for the spectral estimates to be retrieved through a transform from equivalent spectral components estimated using the signal subspace. The 2D ESPRIT algorithm is presented next with a flow diagram shown in Figure 3.2

1. The M x N data matrix $\boldsymbol{Y}$ undergoes polar reformatting through the relationships in Equation 3.5.
2. An orthonormal basis for the underlying vector space $\boldsymbol{U}_T$ is estimated by either
   (a) Estimating the autocorrelation matrix $\boldsymbol{R}$ followed by eigendecomposition and spatial smoothing, or
   (b) Re-arranging the data matrix $\boldsymbol{Y}$ into a Block-Hankel structure and then computing the SVD.
3. The matrix $\boldsymbol{U}_T$ is then partitioned into signal $\boldsymbol{U}$ and noise subspaces $\boldsymbol{U}_{noise}$

$$\boldsymbol{U}_T = \left[\boldsymbol{U} \;\middle|\; \boldsymbol{U}_{noise} \right] \tag{3.10}$$

This partitioning (stripping away of the noise) is done by retaining the P columns of $\boldsymbol{U}_T$ whose corresponding eigenvalues are considered significant.

4. By removing specific rows from $\boldsymbol{U}$, as shown in Burrows [25], it is possible to create three staggered matrices $\boldsymbol{U}_{ref}$, $\boldsymbol{U}_1$ and $\boldsymbol{U}_2$ with matrix pencils ($\boldsymbol{U}_{ref}$,$\boldsymbol{U}_1$) and ($\boldsymbol{U}_{ref}$,$\boldsymbol{U}_2$). These matrices span different, though related subspaces through the rotation operator matrices $\boldsymbol{\Psi}^{\alpha}$ and $\boldsymbol{\Psi}^{\beta}$

$$\begin{aligned} \boldsymbol{U}_1 &= \boldsymbol{U}_{ref}\boldsymbol{\Psi}^{\alpha} \\ \boldsymbol{U}_2 &= \boldsymbol{U}_{ref}\boldsymbol{\Psi}^{\beta} \end{aligned} \tag{3.11}$$

which are estimated here using a least squares projection

$$\begin{aligned} \boldsymbol{\Psi}^{\alpha} &= (\boldsymbol{U}_{ref}^{H}\boldsymbol{U}_{ref})^{-1}\boldsymbol{U}_{ref}^{H}\boldsymbol{U}_1 \\ \boldsymbol{\Psi}^{\beta} &= (\boldsymbol{U}_{ref}^{H}\boldsymbol{U}_{ref})^{-1}\boldsymbol{U}_{ref}^{H}\boldsymbol{U}_2 \end{aligned} \tag{3.12}$$

where a total least squares approach can also be used.

5. The P scattering centres co-ordinates in Cartesian space are then estimated through eigendecomposition of the rotation matrices for this coupled eigenvalue problem

$$\begin{aligned} \hat{\boldsymbol{x}} &= \frac{X_{max}\angle\boldsymbol{\phi}(\alpha)}{2\pi} \\ \hat{\boldsymbol{y}} &= \frac{Y_{max}\angle\boldsymbol{\phi}(\beta)}{2\pi} \end{aligned} \tag{3.13}$$

where vectors $\boldsymbol{\phi}(\alpha)$ and $\boldsymbol{\phi}(\beta)$ contain the the eigenvalues of $\boldsymbol{\Psi}^{\alpha}$ and $\boldsymbol{\Psi}^{\beta}$ respectively and X_{max} and Y_{max} are defined in Table 3.1.

6. One approach to pairing the eigenvalues in Equation 3.13 is to make use of the the eigenvector matrix $\boldsymbol{T}$ of the weighted matrix sum $\alpha_1\boldsymbol{\Psi}^{\alpha} + \alpha_1\boldsymbol{\Psi}^{\beta}$ with $\alpha_1 + \alpha_2 = 1$. In this approach, the pairing is achieved by directly matching the diagonal elements of the matrices $\boldsymbol{T}^{-1}\boldsymbol{\Psi}^{\alpha}\boldsymbol{T}$ and $\boldsymbol{T}^{-1}\boldsymbol{\Psi}^{\beta}\boldsymbol{T}$.

7. The amplitudes of the estimated scattering centres can then be solved through the use of a least squares approach directly through Equation 3.1.

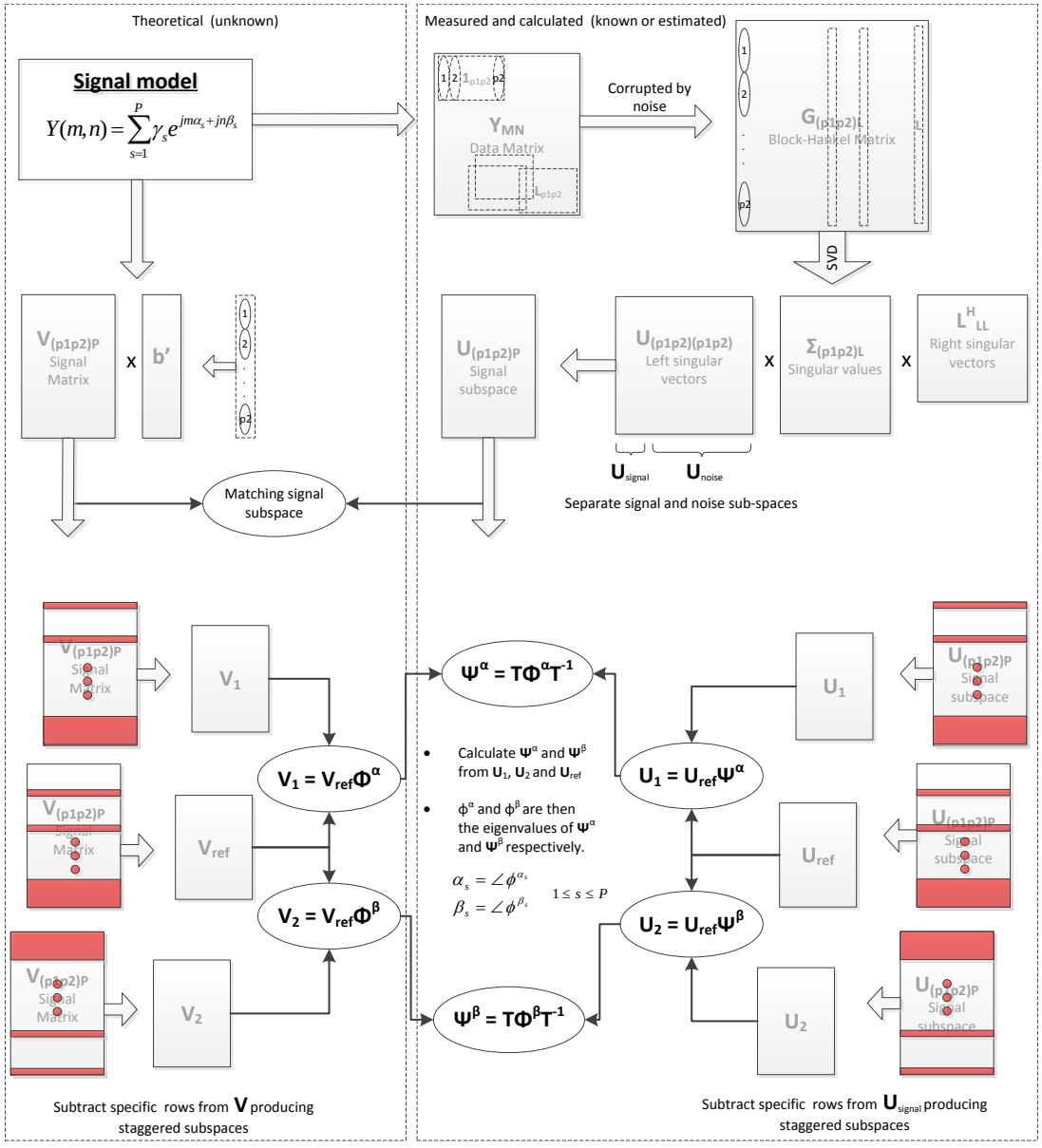

Figure 3.2: Flow diagram of 2D ESPRIT.

3.4 Performance Metrics

The performance metrics that follow are used to evaluate the scattering centre extraction algorithms.

Resolution:

The definition of resolution as defined by Rihaczek and Hershkowitz [27] is used in this study:

Two scatterers are said to be resolved if we are able to perform meaningful positional measurements.

It is then clear, according to this definition, that detecting the correct number of scattering centres alone does not imply that all have been resolved in a manner where the estimated locations relate directly to the source of the scattering.

Measurement precision:

Defines the accuracy of the estimated scattering centre's location and amplitude relative to the true location and amplitude. The root-mean-square error (RMSE) is used to calculate the error between the known and estimated location and a percentage error to quantify the amplitude error

$$error_{amplitude} = \frac{\hat{a} - a}{a} \tag{3.14}$$

In this study, a global nearest neighbour association routine was chosen to associate estimated scattering centers with the known sources. This routine makes use of an Auction algorithm where the sum of all associated distance errors is minimised.

RCS re-synthesis:

Compares the source RCS data with the RCS calculated by reconstructing the scattered field data E_s from the scattering centre estimates through Equation 3.1. The RCS is then determined according to the IEEE definition as given in [28], by

$$RCS = \lim_{R\to\infty} 4\pi R^2 \frac{|E_s|^2}{|E_i|^2} \tag{3.15}$$

where E_i is the incident electric field and E_s the scattered field at a distance R from the observation point. For the current investigation both E_i and R are set equal to 1 while the assumption is still made that R is far enough from the target to avoid near-field effects.

3.5 Summary

In this chapter an overview of the models, mathematical techniques and algorithms employed in this study is presented. The ideal point scatterer model is presented in Section 3.1 with its corresponding small angle approximation presented in Section 3.2. Section 3.2 also presents the relationship between 2D high resolution radar imaging and the 2D spectral estimation problem. Two known spectral estimation techniques, ESPRIT and EP-based CLEAN with their corresponding algorithms, are presented in Section 3.3. The performance metrics used to evaluate the two techniques are presented in Section 3.4.

Chapter 4

Model Development

The extension of ESPRIT to high resolution radar imagery requires the following data pre-processing steps in order to make direct use of the ESPRIT algorithm:

1. Polar reformatting: This is required to present the data in a uniform Cartesian grid which ensures a translation invariance between overlapping subsets of the data matrix.

2. Spatial smoothing: This is required to form different linear combinations of the same spectral components and correspondingly restore the rank of the covariance matrix.

This chapter presents both an analysis of the influence these data pre-processing steps have on the effectiveness of ESPRIT as well as a new technique aimed at mitigating their influence. The influence will be shown to limit operation in one of two ways:

1. The first is noise-limited operation where the noise component of the input data limits achievable performance.

2. The second is processing-limited operation where the data processing or pre-processing limits achievable performance.

4.1 Model Mismatch and Polar Reformatting

The signal model for a two-dimensional spectral estimation problem is given by

$$Y(m,n) = \sum_{s=1}^{P} \gamma_s \exp(jm\alpha_s + jn\beta_s) \tag{4.1}$$

for P components with amplitudes γ_s and independent (i.e. no coupling) frequency components α_s and β_s.

While the small angle approximation of Equation 3.2 is matched to that of Equation 4.1, the ideal point scatterer model of Equation 3.1 is slightly mismatched. This mismatch is caused by the coupling of frequency and aspect angle.

In order to match the measured data, which is in the form of Equation 3.1, to that of Equation 4.1, a polar reformatting of the data is required. Conventionally polar reformatting is achieved through interpolation of measured data with techniques such as nearest neighbour, bilinear or cubic spline interpolation into a uniform Cartesian grid. The new sample points are calculated using Equation 3.5.

The influence of polar reformatting on ESPRIT can be demonstrated through an analysis of the eigenvalues of the covariance matrix where the following attributes of the eigendecomposition of the covariance matrix should be taken into account.

1. The amplitudes of the eigenvalues, whose corresponding eigenvectors span the noise subspace, are directly related to the noise power in a given dimension of the vector space. These amplitudes are equal when an infinite number of samples is used to estimate the covariance matrix and unequal when a finite number of samples is used.

2. The amplitudes of the eigenvalues whose corresponding eigenvectors span the estimated signal subspace are also corrupted by a noise component.

The first point noted above is demonstrated via an illustrative example in Figure 4.1, where a finite number of samples is used to generate the covariance

matrix and the input SNR is varied from 5 to 250 dB. The influence of polar reformatting is decoupled through the proposed technique in Section 4.2, given that the exact location and amplitude of each scattering centre is known.

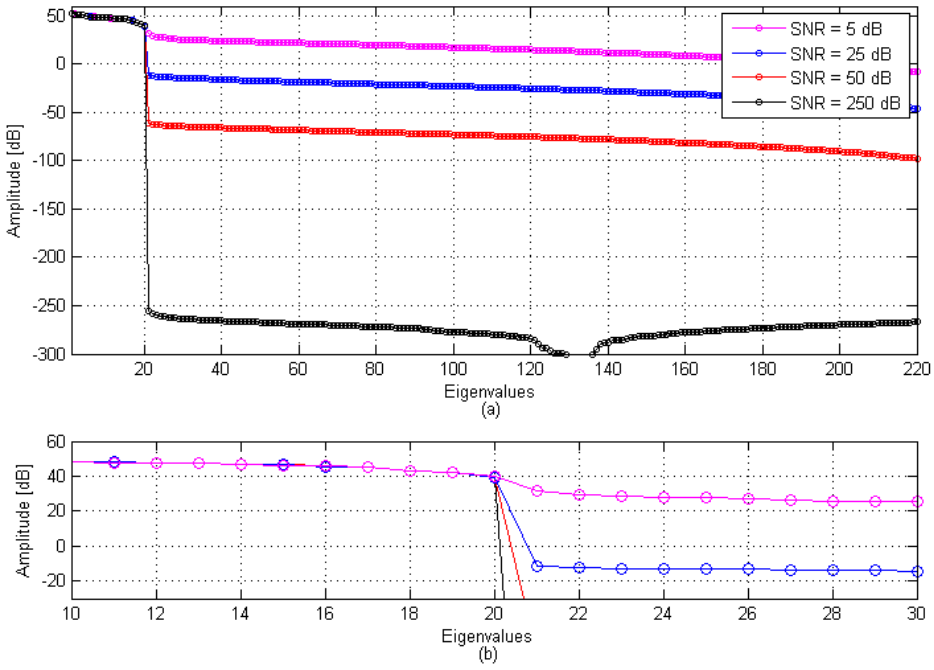

Figure 4.1: Eigenvalues of the covariance matrix as a function of SNR for 20 well defined scattering centres.

The influence of polar reformatting can then be demonstrated through a second illustrative example as presented in Figure 4.2. In Figure 4.2 the eigenvalues of the covariance matrix with no polar reformatting, ideal polar reformatting and interpolation-based polar reformatting is presented.

From the illustrative example of Figure 4.2 the following emerging properties are observed.

1. When no polar reformatting is applied a large percentage of the vector space, corresponding to eigenvalues ranging from 21 to 169 in this example, is spanned by a set of partially correlated spectral components.

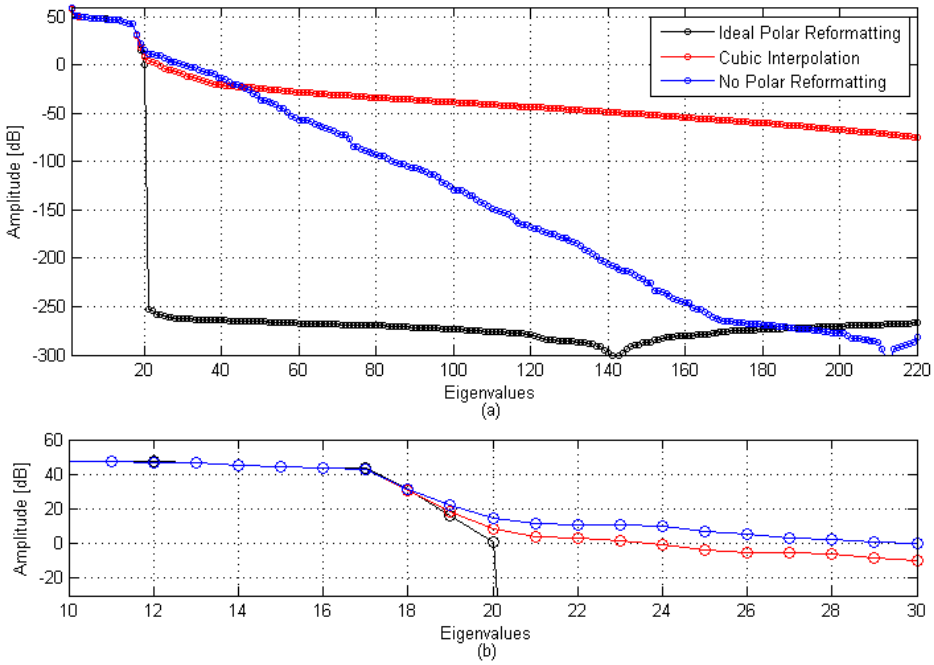

Figure 4.2: A comparison of the eigenvalues of the covariance matrix for Ideal polar reformatting, cubic interpolation and no polar reformatting for SNR = 250 dB.

2. When using interpolation based polar reformatting,

   (a) The larger percentage of the vector space, corresponding to eigenvalues ranging from 45 to 220 in this example, exhibit characteristics similar to that of increasing noise power (decreasing SNR as shown in Figure 4.1).

   (b) A small percentage of the vector space, corresponding to eigenvalues ranging from 21 to 44 in this example, exhibit characteristics similar to that observed when no polar reformatting was applied.

These attributes highlight that interpolation based formatting both introduces noise and fails to perfectly decouple frequency from aspect angle. This is demonstrated by an apparent reduction in SNR and residual partially correlated spectral components. The direct influence these attributes have on ESPRIT is evident

by a more complex split between the signal and noise subspace as well as a reduction in performance as a result of an increase in noise power. These attributes will also reduce the performance of other super-resolution techniques, such as MUSIC.

4.2 An Iterative Approach to Polar Reformatting

In an attempt to mitigate the processing-limited characteristic, found in the current extension of ESPRIT to high resolution radar imagery, an iterative polar reformatting approach was developed based on the following assumption.

For a given scene, should the parameters of all the scattering centres be known a-priori polar reformatting should be possible, without re-sampling and interpolation, directly through the relationships with the ideal point scatterer model. As a result of the influence polar reformatting has on the accuracy of the estimates, an iterative approach can then be implemented where improving the estimates on each step, leads to improved polar formatting, and consequently improved estimates on subsequent steps. However, should the estimates not provide improved polar reformatting, the quality of the estimates can deteriorate over iterations.

In the proposed approach the ideal point scatterer model is mapped to its small angle approximation through a correction vector. This correction vector is calculated from estimates of the scattering centres at each iteration and subtracted from each cell in the data matrix as shown in Equation 4.2.

$$\begin{aligned} E^s_{cart}(m,n) = \sum_{i=1}^{P} \Bigg(& E^s(m,n) + \hat{a}_i \exp(j\frac{4\pi}{c}[f_m\hat{x}_i + f_c\phi_n\hat{y}_i]) \\ & -\hat{a}_i \exp(j\frac{4\pi f_m}{c}[\cos(\phi_n)\hat{x}_i + \sin(\phi_n)\hat{y}_i]) \Bigg) \end{aligned} \tag{4.2}$$

where $\hat{x}$, $\hat{y}$ and $\hat{a}$ are the estimated parameters from the previous iteration. Given that each correction vector comprises a sum of correction vectors for each spectral component the exclusion of specific scatterers results in their contributions remaining coupled within the data.

Initialisation is an important step in the iterative polar reformatting approach. Poor initial estimates can result in poor de-coupling of frequency and angle resulting in a divergence of the results. One approach is to make use of EP-based CLEAN to extract scattering centre estimates for initialisation. EP-based CLEAN is robust against noise and its use of the ideal point scatterer model means that even using residual scattering centers (residual from imperfect cancellation on previous iterations) can improve the quality of the correct vector.

Terminating the algorithm is the second important step in the iterative polar reformatting approach. One approach, that can be used when making use of ESPRIT, is to evaluate the eigenvalues of the noise subspace in the following manner.

1. Diverging (unfavorable) results are identified by amplitudes of the eigenvalues of the noise subspace which increase between each iteration.

2. Converging (favorable) results are identified by amplitudes of the eigenvalues of the noise subspace which decrease between each iteration.

3. Limited improvement is shown by amplitudes of the eigenvalues of the noise subspace which remain constant between each iteration.

4.3 Dividing the Vector Space

Given that the AIC and MDL implementations, proposed by Max and Kailath [13], do not account for introduction of partially correlated spectral components in non ideal polar reformatting, this study makes use of a gradient based approach to separate the signal and noise subspaces. In this approach the local gradient between each eigenvalue, in relation to its amplitude, is used to generate a response where peaks indicate distinct changes. The resulting algorithm is given by

$$\hat{P} = \max_{1 \leq i \leq I} \; log_{10}\left((\frac{\lambda_i}{\lambda_{max}})^{10}\right) - log_{10}\left((\frac{\lambda_{i+1}}{\lambda_{max}})^{10}\right) \tag{4.3}$$

where λ_i is the i^{th} eigenvalue arranged in descending order $\lambda_i > \lambda_{i+1} > ... > \lambda_I$.

This function is expected to produce a distinct peak when a clear separation between signal and noise subspace exists. An illustrative example of this characteristic is shown in Figure 4.3.

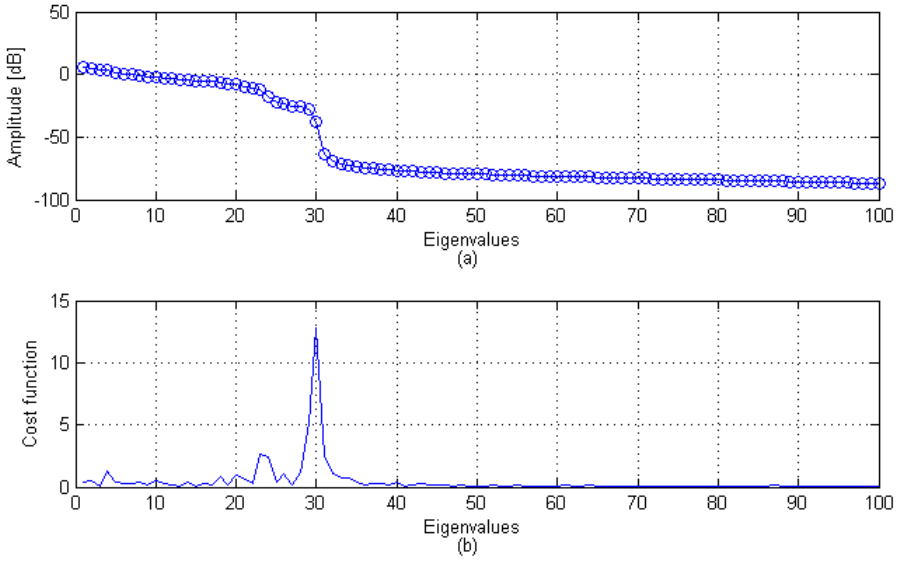

Figure 4.3: Gradient approach demonstrating well defined split between signal and noise subspace for a 30 scatterer scenario.

However, when the region surrounding the correct split is more complex the peak is broken up into smaller less well defined peaks. A second illustrative example highlighting this characteristic is shown in Figure 4.4.

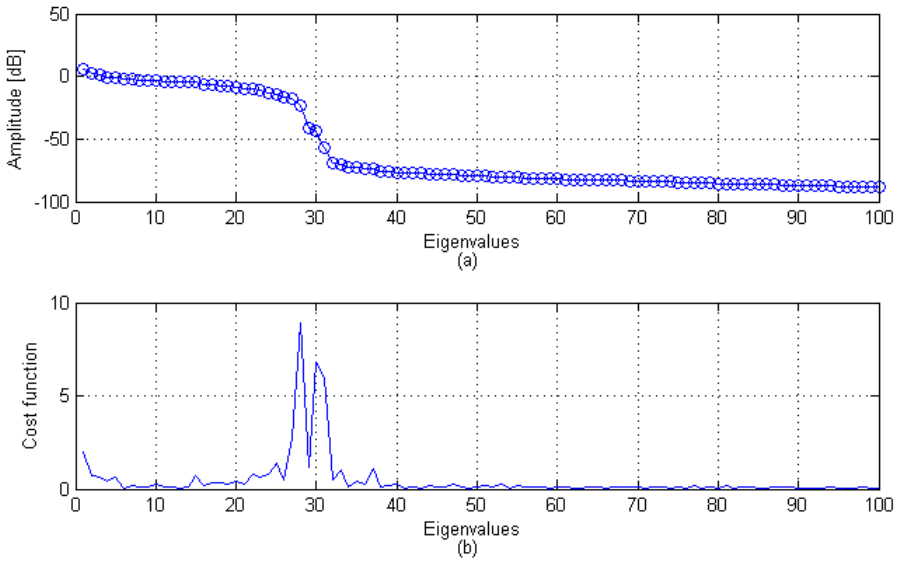

Figure 4.4: Gradient approach demonstrating demonstrating complex split between signal and noise subspace for a 30 scatterer scenario.

When the broken peaks extend slightly past the true number of scattering centres, the inclusion of eigenvectors corresponding to the noise subspace results in reduced performance. For this study this issue was addressed through reducing $\hat{P}$ in an iterative manner, via a threshold on the amplitude estimates.

4.4 Summary

In this chapter an analysis of the performance limiting attributes of the extension of ESPRIT to high resolution radar imagery is presented. The influence of polar reformatting on the operation of ESPRIT is demonstrated in Section 4.1, followed by the development of an iterative polar reformatting technique in Section 4.2. A gradient approach for dividing the signal and noise subspace is then presented in Section 4.3.

Chapter 5

Experimental Methods

The research methodology chosen for this study combines experimental research with some exploratory components. The study makes use of FEKO and Matlab simulations for data collection, interpretation and visualization.

Establishing a preferred approach to decomposing high resolution radar images into sparse representations of point sources, is the primary focus of this study. Emphasis is placed on application in controlled environments where certain parameters are known or controlled. Environments that can be categorized as controlled include high fidelity simulations or compact range measurements.

In order to achieve this objective, a performance comparison between EP-based CLEAN and ESPRIT is presented. Given that the scope of this study does not accommodate an exhaustive comparison, emphasis is placed on the performance as a function of emerging properties. Some preliminary results from an iterative polar reformatting technique developed during this study are also presented.

5.1 Research Questions

In order to achieve the objectives set out in the study the following set of research questions were defined:

Research Question 1: What is the performance of each technique in terms of:

1. Resolution as a function of scatterer amplitude.
2. Measurement precision (i.e. estimated position and amplitude) as a function of SNR.

Research Question 2: Does the proposed iterative polar reformatting technique improve measurement precision?

Research Question 3: Do the techniques produce similar results when comparing data generated through the ideal scattering model (Matlab) and data more representative of true scattering generated using FEKO?

Research Question 4: What is the relationship between extracted scattering centres as a function of aspect angle for the two techniques?

Research Question 5: How do the techniques compare in terms of RCS resynthesis using the extracted scatterers?

5.2 Experimental Configurations

In order to answer the questions put forward, several experiments comprising scenarios with a small number of well defined scattering components were performed. Matlab was used to perform the required processing, through a number of functions developed during the study in a scripting approach, to extract the scattering centres. The experimental configurations are defined next with corresponding results presented in Chapter 6.

5.2.1 Imaging Parameters

The investigations considered in this study are limited to simple distributions of scattering centers in small scenes (<= 5 m^2). The radar imaging parameters are kept constant for each experiment in order to maintain consistency in the results and are presented in Table 5.1.

Table 5.1: Simulation imaging parameters

Radar Parameters	
Centre frequency	10 GHz
Bandwidth	600 MHz
Frequency steps	31
Look angle	3 deg
Angle steps	31
Polarisation	VV

Imaging Properties		
	Cross range [m]	Slant range [m]
Maximum unambiguous range	7.5	8.6
Resolution cell size	0.25	0.29

5.2.2 Research Question 1

Purpose :

In response to Research Question 1 the following investigation aims to compare the two techniques in terms of resolution and measurement precision. While related, the comparisons are presented in a decoupled manner in order to highlight the emerging properties. The investigation therefore comprises two components.

1. The first part of this investigation aims to determine the resolution of each technique.

2. The second part of this investigation makes use of the resolution constraints to define a set of Monte Carlo simulations for resolvable scattering centres that derive the measurement precision as a function of SNR.

Setup :

1. In the first part of this investigation, scattered field data is generated through the ideal scattering centre model in Matlab. The investigation makes use of the imaging parameters from Table 5.1 and a geometry comprising two scattering centres separated in cross range only. One scatterer remains stationary while the separation between the scatterers is reduced on each iteration. This is repeated for amplitude ratios of -20, -40 and -60 dB.

   Ideal polar reformatting is applied to the data through Equation 4.2 with the known scattering center parameters. The resolution performance of ESPRIT is then quantified through analysis of the eigenvalues of the covariance matrix. Using the relationships between signal and noise subspaces, two scatterers are termed resolvable until the amplitude of the second eigenvalue equals that of the third eigenvalue (first eigenvalue associated to the noise subspace).

   The analysis for EP-based CLEAN considers amplitude ratios of 0, -10, -30 and -60 dB with the same geometry configuration used with ESPRIT. However, only the resolution upper bound (functional resolution by Rihaczek and Hershkowitz [27]) is evaluated in this study. This implies zero phase difference between interfering scattering centers.

   This approach was followed as a result of the sensitivity of the CLEAN class of algorithms to the interference characteristics of two scatterers. This sensitivity is highlighted by Rihaczek and Hershkowitz [27] where the resulting structure from two interfering sources with constant separation, is shown to vary from two well defined peaks to a single peak by only changing the phase difference.

2. For the second part of this investigation, sets of scattering centres were generated from a uniform distribution that span the unambiguous cross and slant ranges of the scene. An example is shown in Figure 5.1.

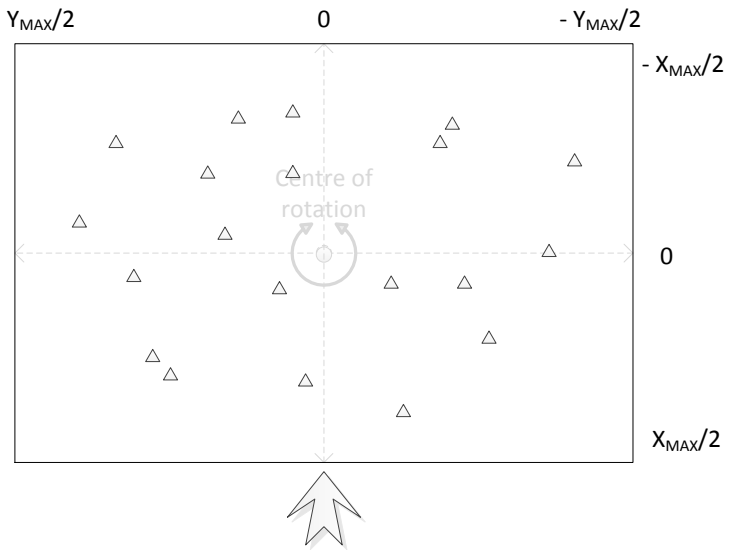

Figure 5.1: Simulation geometry: Sparse distribution of scatterers.

Scattering centres separated by a distance closer than that required for resolvability over all SNR were replaced by new samples from the same distribution. For this study SNR is defined as the ratio of signal power to noise power prior to any signal processing. The scattered field data was generated using the ideal point scatterer model in Matlab. The parameters for the analysis are presented in Table 5.2.

Table 5.2: Simulation parameters for measurement precision comparison.

Parameter	Value(s)
Closest separation [m]	0.5
Number of scatterers	20
Monte Carlo runs	500
Location error metric	RMSE
Amplitude error metric	Percentage error
Association	Global nearest neighbour (Auction algorithm)
SNR values [dB]	0, 2.5, 5, 10, 15, 20, 35, 50, 100 and 250

5.2.3 Research Question 2

Purpose :

In response to Research Question 2, the following investigation aims to verify whether an iterative approach to polar reformatting is able to improve the accuracy of the estimated scattering centres using ESPRIT.

Setup :

For the current investigation scattered field data is generated using the same setup as defined in Research Question 1, Setup 2. The investigation makes use of the imaging parameters from Table 5.1 as well as investigation specific parameters defined in Table 5.3.

5.2.4 Research Question 3

Purpose :

In response to Research Question 3, the following investigation aims to verify whether scattering centre extraction from synthetic data derived by CEM produces similar results compared with data generated from the ideal point scatterer model.

Table 5.3: Simulation parameters to evaluate iterative polar reformatting.

Parameter	Value(s)
Closest separation [m]	0.5
Number of scatterers	50
Number of ESPRIT iterations	60
Monte Carlo runs	50
Location error metric	RMSE
Association	Global nearest neighbour (Auction algorithm)
SNR values [dB]	50, 150 and 250

Setup :

Caner [1] shows that, over limited angular sectors, the backscattered EM field from dihedrals exhibit ideal point scattering characteristics. Based on this characteristic, a geometry comprising three dihedrals as shown in Figure 5.2 was chosen to generate synthetic data in FEKO.

Given that each dihedral consists of several edges, it is expected that the edges will also exhibit point like scattering (i.e. edge diffraction). As a result of using vertically polarized planar waves the contribution from the top and bottom edges of the dihedrals is assumed negligible; however, the scattering from the front vertical edges is assumed to be significant. The expected set of scattering centres for this geometry is summarised in Table 5.4 where the X and Y axis translate to slant range and cross range respectively. The values used for the expected amplitudes were chosen based on outputs from initial FEKO simulations.

An equivalent scattered field data set was generated in Matlab using the parameters in Table 5.4. This was done in order to directly compare the results from FEKO to the ideal point scatterer results generated in Matlab. Both Matlab and FEKO simulations made use of the same imaging parameters of Table 5.1 where the SNR for the ideal model data was set at 300 dB.

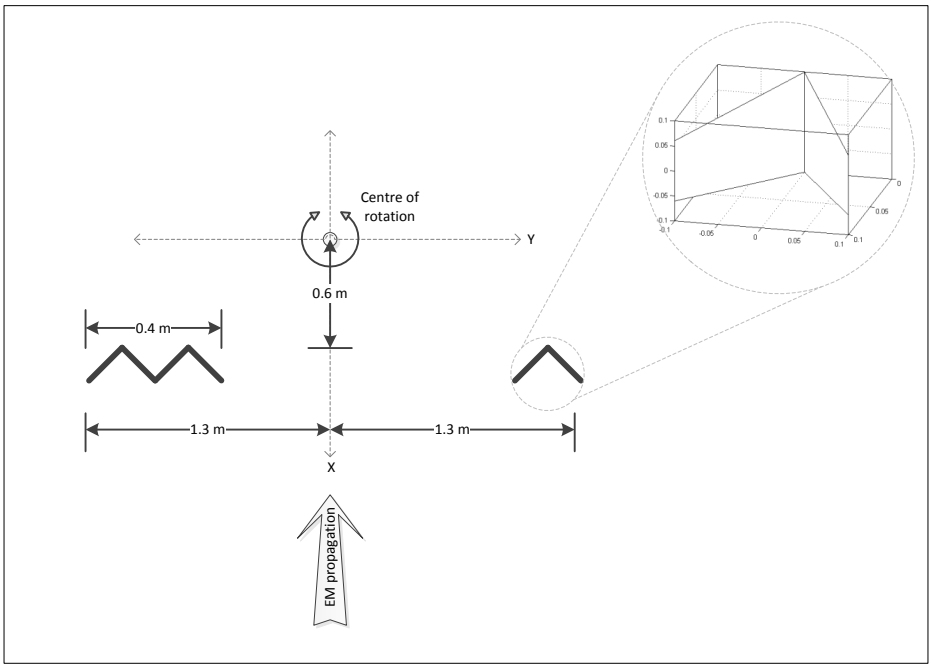

Figure 5.2: Simulation geometry: Three dihedral configuration in FEKO.

Table 5.4: Expected scattering centre locations and amplitudes for three dihedral scenario.

Expected point scatterer attributes		
X [m]	Y [m]	Amplitude
0.7	-1.3	0.025
0.6	-1.2	0.5
0.7	-1.1	0.025
0.6	-1	0.5
0.7	-0.9	0.025
0.7	1.1	0.025
0.6	1.2	0.5
0.7	1.3	0.025

5.2.5 Research Question 4

Purpose :

Given that the same scattering source may produce localised radiation over a large scene rotation the ability to associate scattering centres from scene to scene as a function of their position and amplitude has inherent value. In response to Research Question 4, this investigation aims to evaluate both ESPRIT and EP-based CLEAN in terms of the relationship between their scattering centre estimates from scene-to-scene as a function of aspect angle.

Setup :

The following investigation makes use of the same FEKO geometry used in Research Question 3. Using the same instantaneous imaging parameters given in Table 5.1, scattered field data was generate over a total look angle of 90 deg which translates to a scene rotation from -45 to 45 deg.

Scattering centre extraction was performed on overlapping angle subsets as shown in Figure 5.3 where no association of scattering centres between scenes is performed.

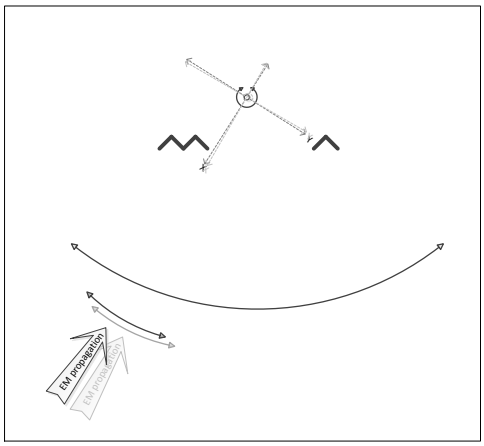

Figure 5.3: Simulation geometry: Overlapping subsets for a 90 deg scene rotation.

5.2.6 Research Question 5

Purpose :

Once estimates of the scattering centres are known, the scattered field can be re-synthesised through the ideal point scatterer model. In response to Research Question 5, this study aims to quantify how well the re-synthesised scattered field matches the original scattered field using estimates from each technique.

Setup :

The current investigation makes use of the data set generated in Research Question 5 where the scattered field data is re-synthesised using the estimated scattering centres through Equation 3.1. The re-synthesised scattered field data is then converted to an RCS value for each frequency and aspect angle through Equation 3.15 and compared to the RCS values generated in FEKO.

The termination requirement on EP-based CLEAN was 100 scattering centres where the largest 10 are used for re-synthesis.

5.3 Summary

In this chapter the approach taken to address the primary objective of this study is presented. Section 5.1 presents the research questions defined in the study where the procedures and experimental configurations used to investigate each research question is presented in Section 5.2.

Chapter 6

Results

The following section presents a compilation of results derived through several investigations performed during this study where each investigation aims to address one of the research questions put forward in Chapter 5. The results were generated from the experimental configurations and procedures also presented in Chapter 5.

6.1 Technique Performance Comparison

The primary purpose of this experiment is to compare the performance in terms of resolution and measurement precision between EP-based CLEAN and ESPRIT.

In evaluating the resolution of ESPRIT, the difference in eigenvalue amplitude as a function of the scattering centre separation for amplitude ratios of 0, -20, -40 and -60 dB is presented in Figure 6.1.a. The corresponding difference in eigenvalue amplitude as a function of SNR between the last eigenvalue associated to the signal subspace and the first eigenvalue associated to the noise subspace is presented in Figure 6.1.b.

In evaluating the resolution of EP-based CLEAN, the RMSE for the primary

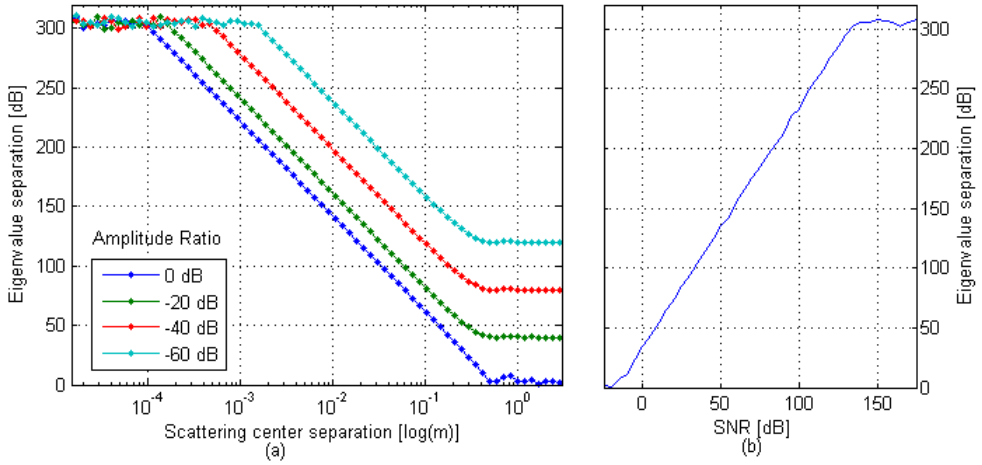

Figure 6.1: ESPRIT scatterer resolving capability in terms of a) required eigenvalue separation as a function of scatterer separation and corresponding b) eigenvalue separation as a function of SNR.

and secondary estimated scattering centres for amplitude ratios of 0, -10, -30 and -60 dB is presented in Figure 6.2.

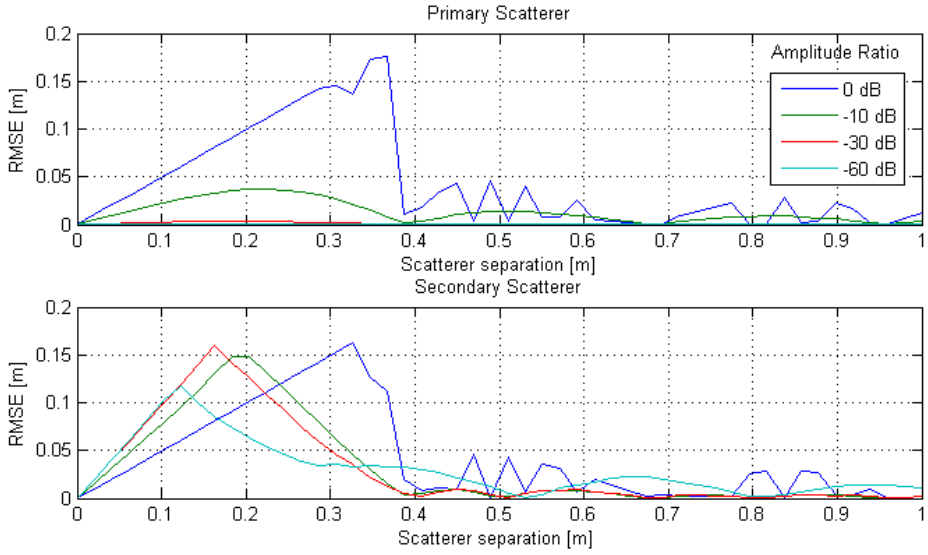

Figure 6.2: RMSE as a function of scatterer separation for EP-based CLEAN with amplitude ratios of 0, -10, -30 and -60 dB.

Figure 6.3 shows the normalized cost function as a function of scatterer separation

used to derive the results presented in Figure 6.2. The images on the left show the initial cost function output and initial estimated primary scatterer location where the images on the right show the cost function output after the first deconvolution step with estimated secondary scatterer location.

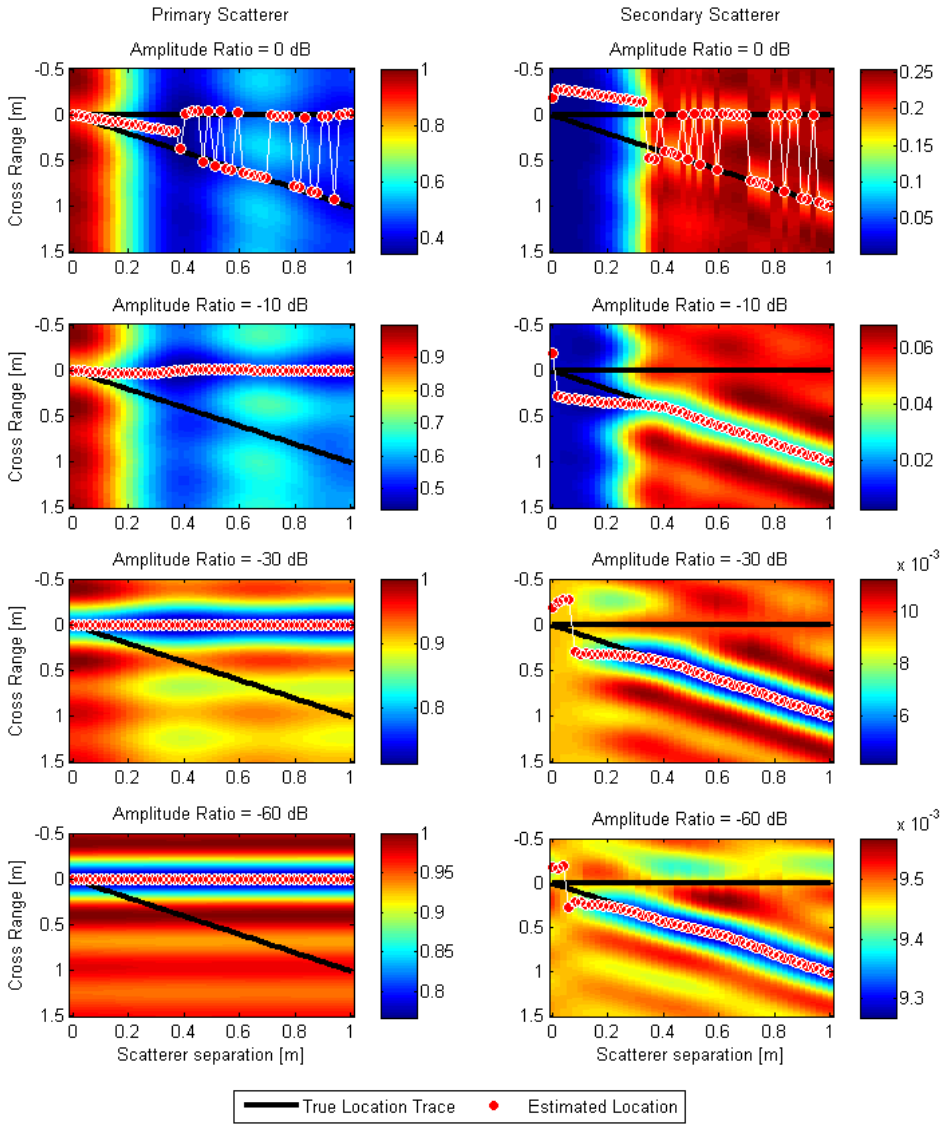

Figure 6.3: EP-based CLEAN cost function output as a function of scatterer separation and amplitude ratio with estimated primary (left) and secondary (right) scattering centres.

In evaluating the measurement precision of EP-based CLEAN and ESPRIT, Figure 6.4.a presents the RMSE error and Figure 6.4.b the amplitude error as a function of SNR for a Monte Carlo simulation comprising 500 iterations.

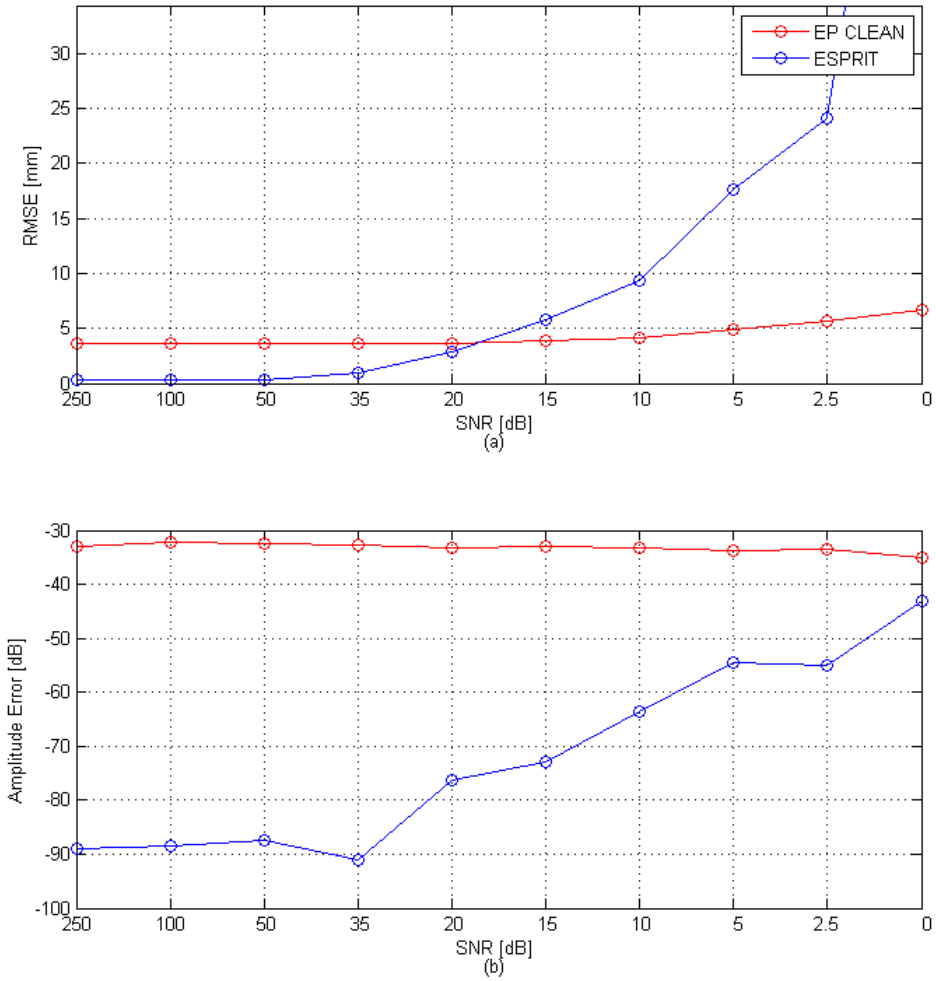

Figure 6.4: Performance comparison: a) RMSE and b) amplitude error as a function of SNR for ESPRIT and EP-based CLEAN through Monte Carlo analysis over 500 iterations.

6.2 Iterative Polar Reformatting

The primary purpose of this investigation is to verify whether the proposed iterative polar reformatting technique, in conjunction with ESPRIT, can improve estimation accuracy.

Using the experimental setup from Research Question 2, a single scene from the Monte Carlo analysis comprising 50 scattering centres is shown in Figure 6.6.

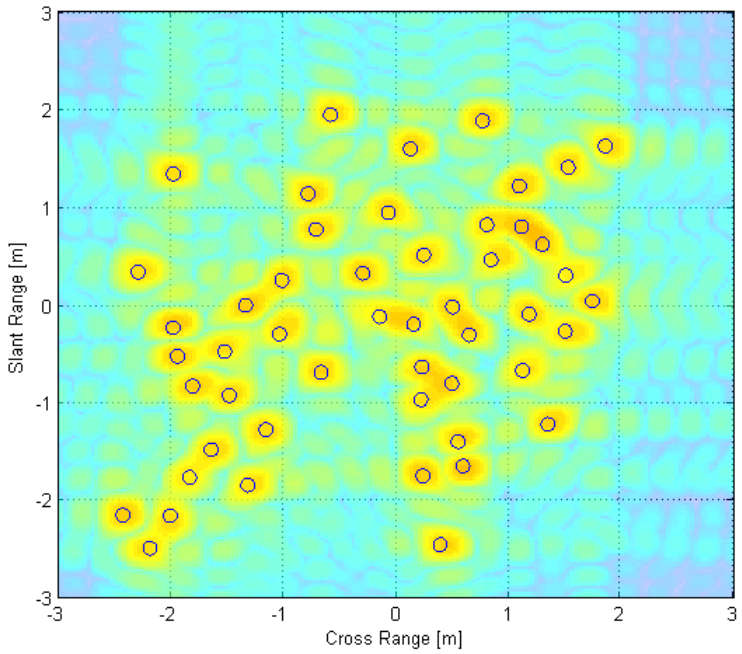

Figure 6.5: Single scene comprising 50 scattering centres from a uniform distribution.

The RMSE error as a function of iteration step, using the ESPRIT estimates to improve polar reformatting, is presented in Figure 6.6. The results present three independent Monte Carlo simulations with SNR values of 50, 150 and 250 dB.

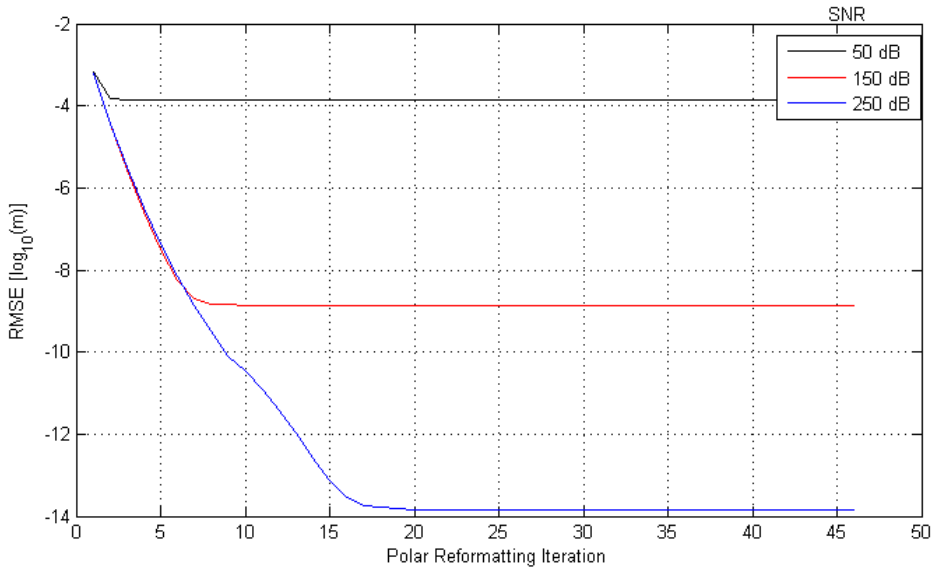

Figure 6.6: ESPRIT estimation RMSE error reduction through iterative polar reformatting using Monte Carlo analysis at SNR values of 50, 150 and 250 dB.

6.3 Ideal Point Scatterer Model Compared to CEM

The primary purpose of this investigation is to provide a comparison between scattering centres extracted using the ideal point scatterer model and data more representative of true EM scattering.

The geometry used to generate the synthetic EM scattered field data in FEKO is shown in Figure 6.7.

Scattering centre estimates from the FEKO data as well as an equivalent data set generated in Matlab using the ideal point scatterer model, are presented in Figure 6.8. Two sets of results for ESPRIT are shown: the first using conventional interpolation based polar reformatting (Cubic spline) and the second using iterative polar reformatting using EP-based CLEAN outputs to seed the process followed by one iteration of ESPRIT.

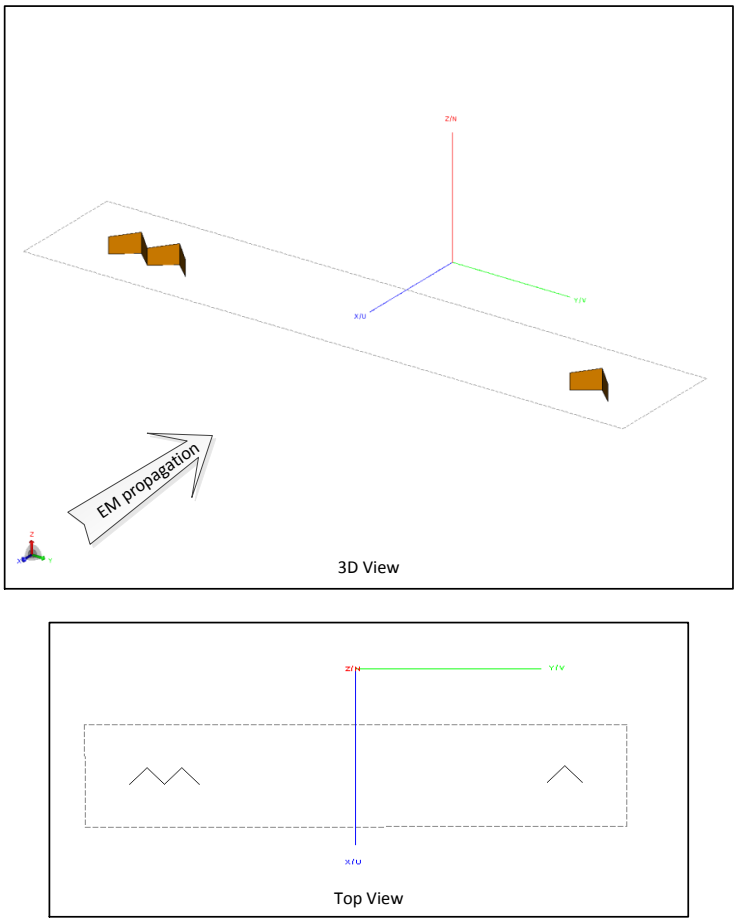

Figure 6.7: Geometry for distributed dihedrals in FEKO.

The eigenvalues corresponding to the two sets of ESPRIT results, for both FEKO and Matlab data sets, are presented in Figure 6.9 followed by a summary of the estimated scattering centres in Tables 6.1, 6.2 and 6.3.

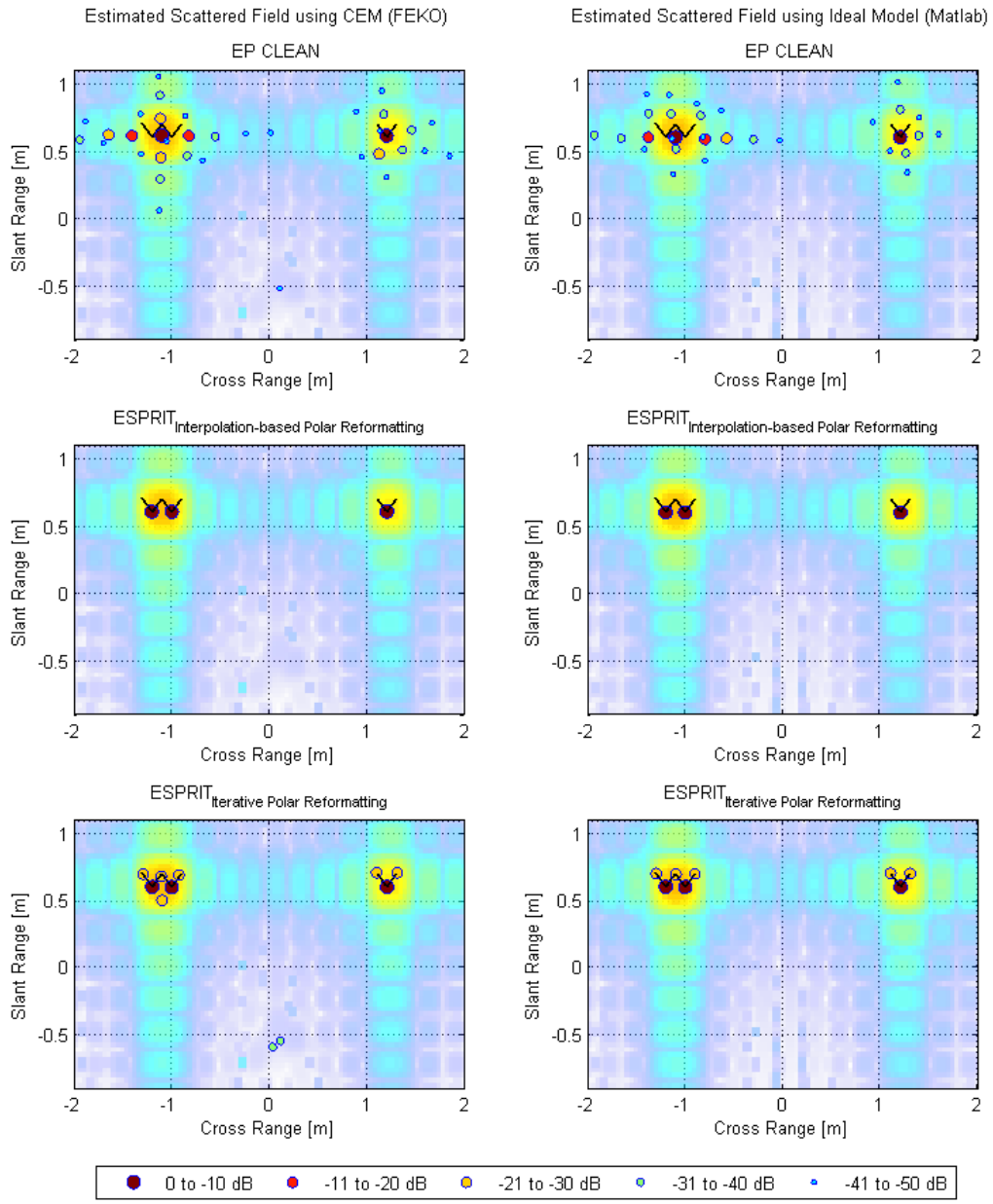

Figure 6.8: Comparison between techniques using scattered field data generated by the ideal point scatterer model (Matlab) and calculated using CEM (FEKO). The dihedral's outline is shown with corresponding extracted scattering centres and FFT based ISAR image overlays.

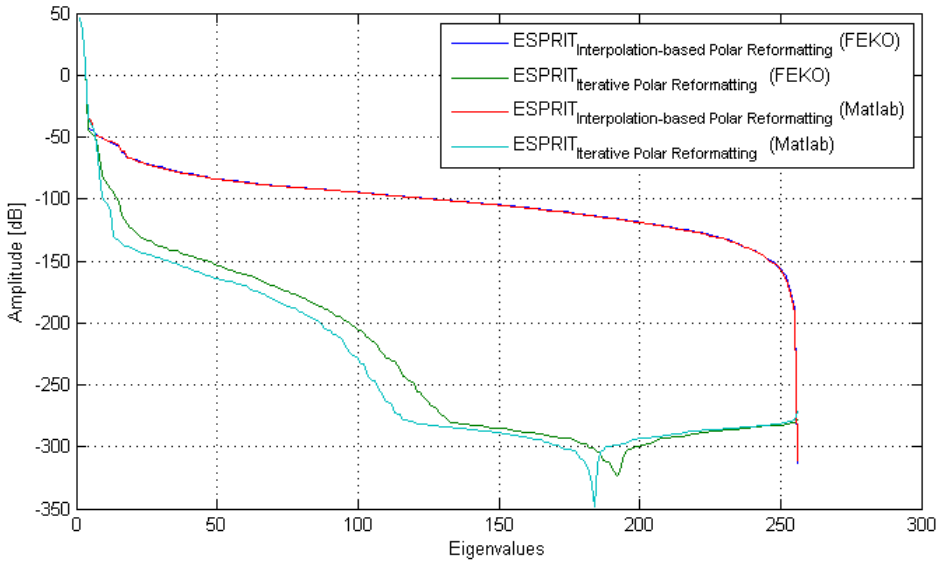

Figure 6.9: Comparing the influence of polar reformatting on the eigenvalues of the covariance matrix for scattered field data generated by the ideal point scatterer model (Matlab) and solved using CEM (FEKO).

Table 6.1: Estimated scattering centres using ESPRIT with interpolation-based polar reformatting.

Dihedral Centres							
Cross Range [m]			Slant Range [m]			Amplitude	
True	Matlab	FEKO	True	Matlab	FEKO	Matlab	FEKO
0.600	0.597	0.603	1.200	1.200	1.200	0.486	0.484
0.600	0.597	0.603	-1.000	-1.003	-1.000	0.486	0.491
0.600	0.598	0.603	-1.200	-1.201	-1.203	0.481	0.479

Table 6.2: Estimated scattering centres using ESPRIT using iterative polar reformatting.

Dihedral Centres							
Cross Range [m]			Slant Range [m]			Amplitude	
True	Matlab	FEKO	True	Matlab	FEKO	Matlab	FEKO
0.600	0.600	0.600	1.200	1.200	1.200	0.500	0.472
0.600	0.600	0.599	-1.000	-1.000	-1.000	0.501	0.471
0.600	0.600	0.600	-1.200	-1.200	-1.199	0.501	0.466
Dihedral Edges							
0.700	0.700	0.705	1.300	1.300	1.306	0.025	0.021
0.700	0.700	0.705	1.100	1.099	1.094	0.025	0.021
0.700	0.698	0.688	-1.000	-0.902	-0.927	0.025	0.024
0.700	0.693	0.678	-1.100	-1.094	-1.109	0.026	0.031
0.700	0.698	0.694	-1.200	-1.296	-1.292	0.026	0.019
Other Estimates							
		0.500			-1.098		0.033
		-0.585			0.032		0.005
		-0.539			0.111		0.005

Given that the EP CLEAN technique does not aim to estimate the number of scattering centres, only the first 10 are considered and presented here. No association is performed given the complex distribution around the expected sources.

Table 6.3: Estimated scattering centres using EP-based CLEAN.

Scattering Centres					
Cross Range [m]		Slant Range [m]		Amplitude	
Matlab	FEKO	Matlab	FEKO	Matlab	FEKO
0.600	0.612	-1.100	-1.101	0.800	0.782
0.600	0.612	1.196	1.196	0.474	0.470
0.585	0.612	-0.798	-1.407	0.115	0.119
0.600	0.612	-1.378	-0.825	0.108	0.113
0.592	0.449	-0.577	-1.112	0.037	0.060
0.482	0.619	1.253	-1.645	0.022	0.039
0.514	0.740	-1.096	-1.114	0.024	0.036
0.774	0.478	-1.145	1.120	0.019	0.026
0.592	0.604	-1.654	-0.556	0.024	0.022
0.585	0.508	-0.302	1.358	0.013	0.021

6.4 Scatterer Trajectories

The primary purpose of this investigation is to compare the relationships between scattering centre estimates, from both EP-based CLEAN and ESPRIT, as a function of small changes in aspect angle across the scene.

The true trajectories of the scattering centres, as a function of slant and cross range for consecutive 0.1 deg rotations of the scene over a 90 deg total look angle (-45 to 45 deg) are shown in Figure 6.10.

From synthetic scattered field data generated in FEKO, the scatterer trajectories as estimated by EP-based CLEAN, ESPRIT using interpolation based polar reformatting and ESPRIT using iterative polar reformatting are shown in Figures 6.11, 6.12 and 6.13 respectively.

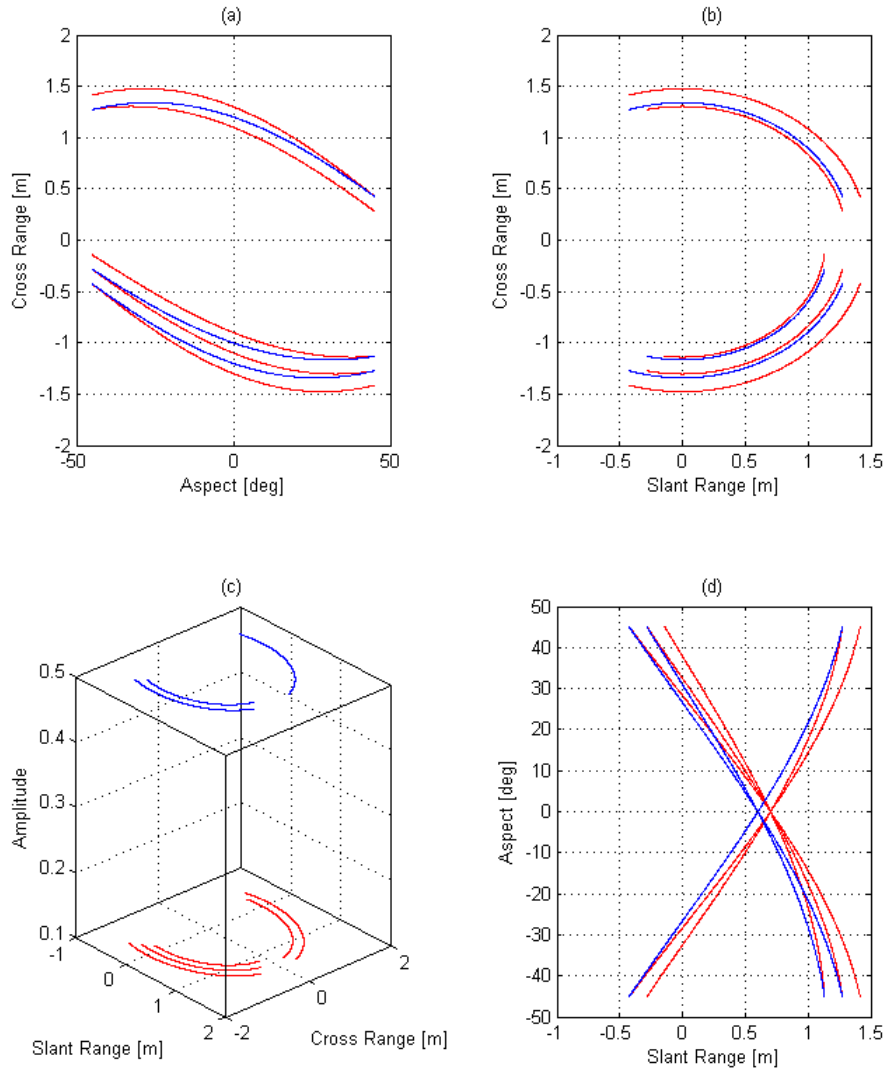

Figure 6.10: True scatterer trajectories over the 90 deg scene rotation as a function of slant and cross ranges. The scattering centres corresponding to each dihedral apex is shown in red with the scattering centres corresponding to each dihedral's edges in blue.

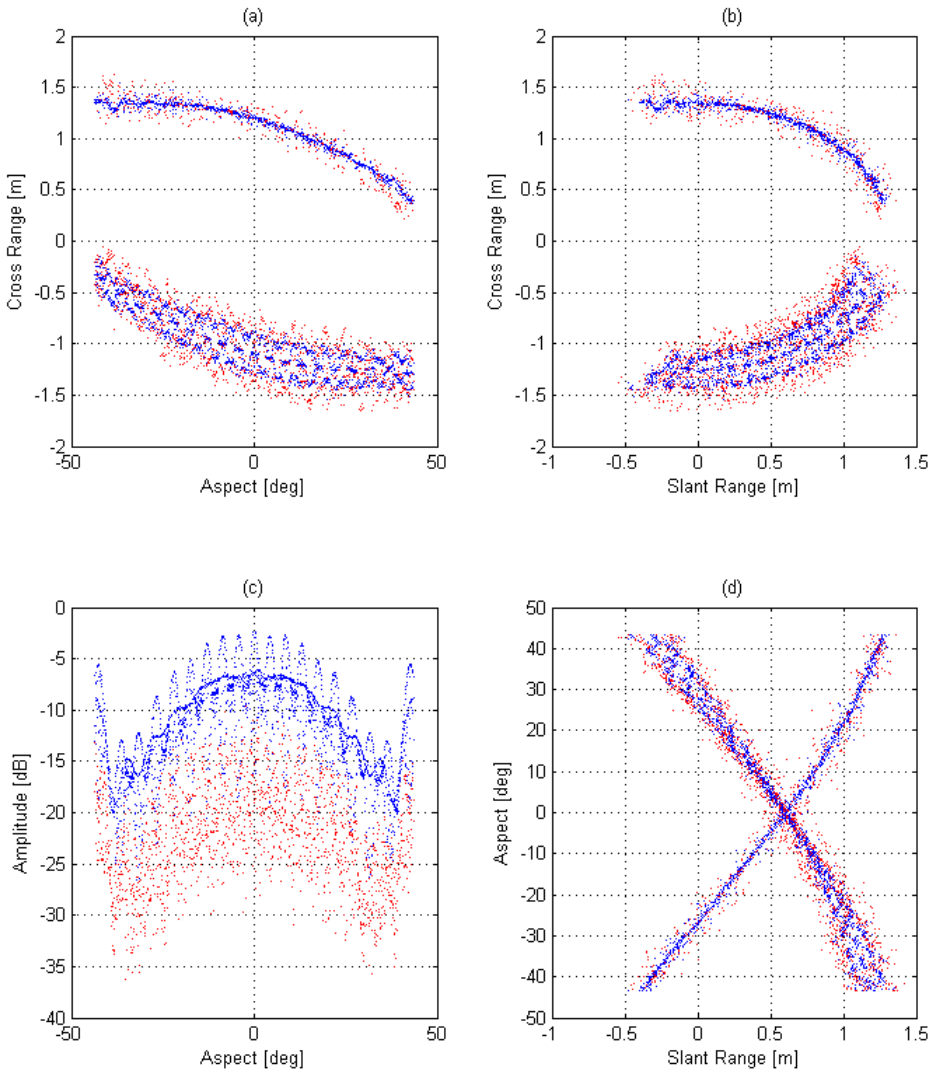

Figure 6.11: Extracted scattering centres using EP-based CLEAN as a function of aspect angle. Scatterers corresponding to the three largest amplitudes at each angle are blue and the remainder in red.

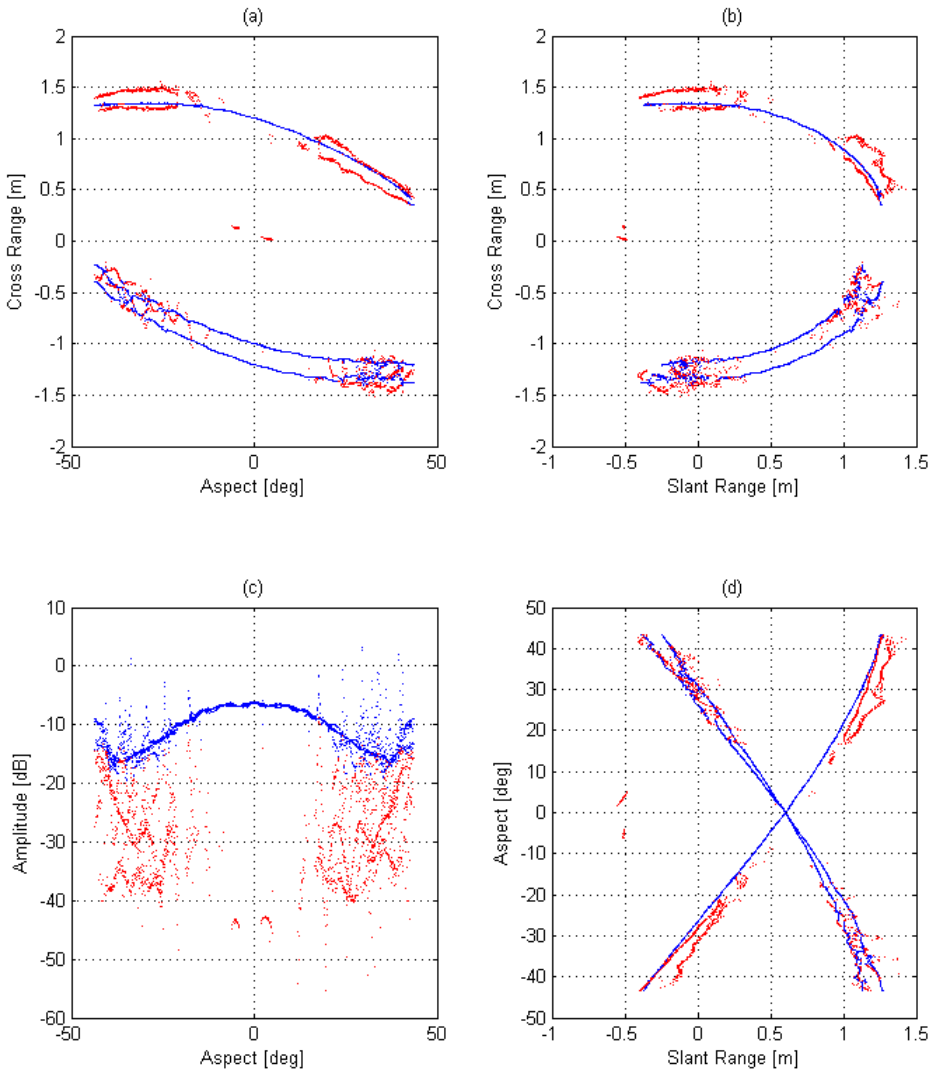

Figure 6.12: Extracted scattering centres using ESPRIT with interpolation-based polar reformatting as a function of aspect angle. Scatterers corresponding to the three largest amplitudes at each angle are blue and the remainder in red.

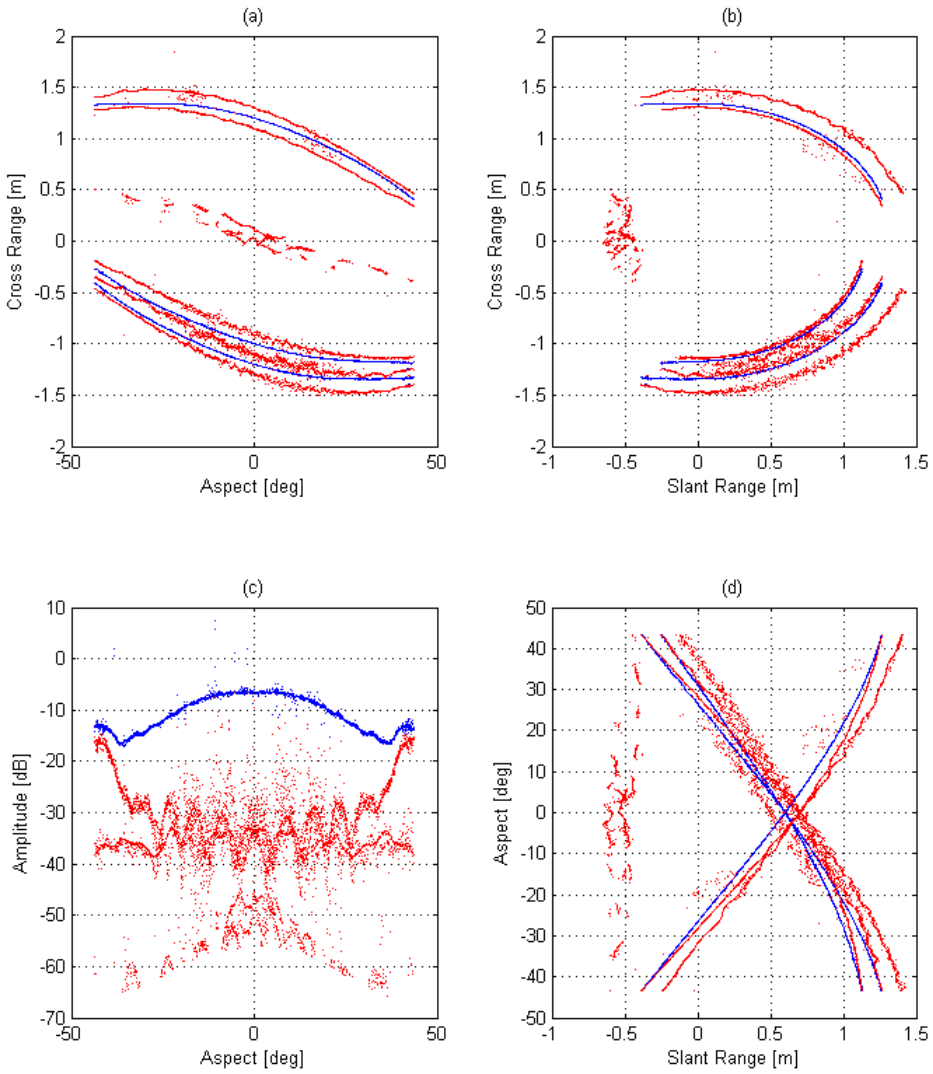

Figure 6.13: Extracted scattering centres using ESPRIT with iterative polar reformatting as a function of aspect angle. Scatterers corresponding to the three largest amplitudes at each angle are blue and the remainder in red.

6.5 RCS Re-synthesis

The primary purpose of this investigation is to evaluate the quality of re-synthesised scattered field data generated using the scattering centre estimates from EP-based CLEAN and ESPRIT.

Figure 6.14.a presents a comparison between the mean (over frequency) RCS value as a function of aspect angle of the FEKO calculated RCS and that calculated from the re-synthesised scattered field data. The RMSE of the re-synthesised RCS, as a function of frequency over aspect angle, compared to the FEKO data is presented in Figure 6.14.b.

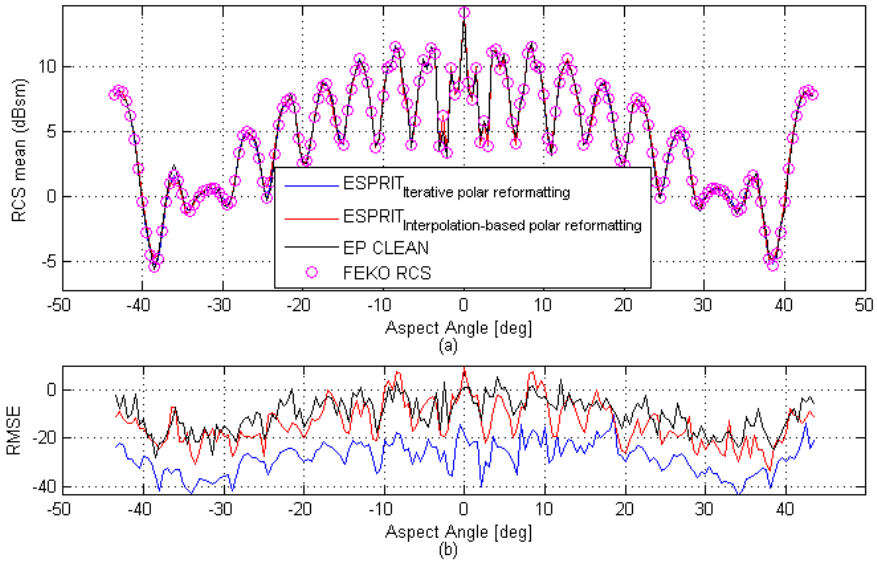

Figure 6.14: Comparison between RCS calculated in CEM and RCS re-synthesised using the extracted scattering centres over a 90 deg scene rotation.

6.6 Summary

In this chapter the results for the experimental configurations described in Chapter 5 are presented. The observed trends are discussed in detail in Chapter 7.

Chapter 7

Discussion and Conclusion

This chapter concludes the study with a discussion of the results presented in Chapter 6, a presentation of high level conclusions reached as well as scope for future work.

7.1 Results Analysis

In this study, two scattering centre extraction techniques are evaluated in terms of their usefulness in controlled environments. A limited performance comparison is presented based on the ideal point scatterer model as well as an evaluation of how the techniques perform when using more representative EM scattering data calculated using CEM methods.

Given the results presented in Chapter 6 and corresponding research questions in Chapter 5 the following subsection presents an interpretation of the results in the context of how each investigation contributes to addressing the primary goal of the study.

7.1.1 Algorithm Resolution

Discussion of results

With no formal definition for achievable resolution in ESPRIT the results presented in Figure 6.1 attempt to quantify the resolution using the eigenvalues of the covariance matrix. As is demonstrated in Figure 6.1.a, a reduction in scatterer separation results in an increase in the amplitude difference of the corresponding eigenvalues. In the same way, increasing SNR results in an increase in the eigenvalue amplitude separation between the signal subspace and the noise subspace as demonstrated in Figure 6.1.b. In this analysis amplitude separation is defined as the difference in the log of the amplitudes.

The results from Figure 6.1.a highlight three resolution regions with distinct characteristics. In the first region, the eigenvalue amplitude difference remains almost constant with a slight lobing structure with peaks that are a function of the separation. This region contains resolvable scattering centres, considered well separated and is defined as the upper bound for resolving two scattering centres. In the second region, the eigenvalue amplitude and scattering centre separation exhibit a logarithmic relationship. This region can be classified as the resolvable sub-resolution-cell region. In the third region, the eigenvalue amplitude separation saturates and is defined as the lower bound for resolving two scattering centres. As demonstrated in Figure 6.1.a, a change in the amplitude ratio of the scattering centres raises the resolution curve and correspondingly changes the upper and lower resolution bounds. These bounds are directly constrained by the SNR which limits achievable eigenvalue separation.

Phase introduced by interfering localised radiation sources influences the interference structure in the cost function of EP-based CLEAN. Given the sensitivity to phase, which varies depending on the mechanism responsible for the scattering, quantifying the resolution for EP-based CLEAN is a difficult task. As a result of this the results presented in Figure 6.2 focuses on the resolution upper bound which assumes that the phases introduced from all localised scattering sources are equal.

The results from Figure 6.2 show the RMSE for the primary (located first) and secondary scattering centres as a function of amplitude ratio. Figure 6.3 presents the cost function and corresponding primary and secondary estimates (following the first deconvolution iteration) from the same set of data.

While smaller errors are observed down to a separation of approximately 0.4 m (≈ 1.5 times the sample resolution) the results show that further reduction results in a increase in the error at a rate directly proportional to the amplitude ratio. For an amplitude ratio of 0 dB, the rate is at its maximum. At this separation, estimated scattering centres are no longer resolved, according to the definition of resolution, given that there is no direct relation to the true locations when considered individually. As the amplitude ratio decreases, the results show that the primary scatterer becomes resolved and a threshold can be applied to the error in the secondary scatterer dictating at what point separation it is no longer defined as resolved.

It appears, from the results for EP-based CLEAN, that resolution improves with decreasing amplitude ratio. This trend is expected to converge at the amplitude ratio at which residual amplitude from imperfect cancellation of the primary scatterer becomes dominant.

Conclusion

The results from EP-based CLEAN have demonstrated a functional resolution of around 1.5 times the sample resolution. In contrast, ESPRIT has demonstrated sub-resolution cell resolving capabilities. In the presence of noise the resolving capabilities of both techniques are reduced. When using EP-based CLEAN, weaker scattering centres can be masked by the noise and as a result are not resolvable, where for ESPRIT partially correlated scattering centers can be masked by the noise and as a result are not resolvable.

7.1.2 Algorithm Measurement Precision

Discussion of results

In order to quantify the measurement precision of EP-based CLEAN and ESPRIT a Monte Carlo analysis comprising 500 iterations was performed. The results are presented in Figure 6.4. The results show that at high SNR the RMSE error for ESPRIT is a factor of 10 times lower than that of EP-based CLEAN. This trend remains constant until a SNR of approximately 50 dB at which point the error begins to increase at a rate faster than that of EP-based CLEAN. The errors are shown to be equal at a SNR of 18 dB after which the RMSE in ESPRIT is larger than that of EP-based CLEAN.

EP-based CLEAN produces a more constant RMSE error over the full range of SNR values considered. This is demonstrated with an RMSE increase of $\approx$ 4 mm as the SNR decreases from 250 to 0 dB. The amplitude error for EP-based CLEAN is also shown to remain almost constant over the same range of SNR values. The amplitude error for ESPRIT, while offering significant performance improvement over the full range of SNR values considered increases as the SNR is reduced. This characteristic is expected given the use of a least squares approach to solve the amplitude estimates using the estimated scatterer locations.

The results for the second Monte Carlo simulation, using the new iterative polar reformatting technique, is presented in Figure 6.6. The results show a clear trend in which the RMSE is reduced to a bound, as a function of SNR, and then offers no further improvement. These bounds are $\approx 1.5 \times 10^{-6}$ m (SNR = 50 dB), 1.5×10^{-9} m (SNR = 150 dB) and 1.5×10^{-14} m (SNR = 250 dB).

Given the results in Figure 6.6, it would seem that the convergence of the measurement precision seen in Figure 6.4 for SNR >= 50 dB is due to being processing limited as a result of using interpolation based polar reformatting. In contrast, the use of iterative polar reformatting achieves a noise-limited performance which is limited only by the input SNR. It is important to note that this analysis only considers uncorrelated scattering centres. In the presence of partially cor-

related scattering centres, the performance gains will be heavily reduced when using only ESPRIT estimates in the iterative approach. This characteristic is expected given that failure to decouple a single scattering center produces a large number of partially correlated spectral components through spatial smoothing.

Conclusion

The results from this investigation have shown that ESPRIT offers improved performance compared to that of EP-based CLEAN in terms of both resolution and measurement precision at high SNR. In addition, when the scattering centres are well separated further performance gains are possible through the use of the proposed iterative polar reformatting technique.

7.1.3 Validation on use of the Ideal Point Scatterer Model

Discussion of results

Computational electromagnetics was used to calculate the scattered field for a simple scenario comprising three dihedrals in FEKO (shown in Figure 6.7). The estimated scattering centres were then extracted using EP-based CLEAN, ESPRIT (interpolation-based polar reformatting) as well as ESPRIT (iterative polar reformatting) and presented in Figure 6.8. The results from a comparative scattered field, generated in Matlab using the ideal point scatterer model and the expected scattering locations, are also shown. For both sets of data, the ISAR image generated using conventional FFT processing is used as an overlay.

A summary of the extracted scattering centres is presented in Tables 6.1, 6.2 and 6.3. In addition, the eigenvalues generated during the ESPRIT processing are presented in Figure 6.9. A summary of the observed trends is given as follows:

1. EP-based CLEAN detects a single scattering centre for the dihedral pair (joined dihedrals) along with residual scattering centres not associated to either dihedral apex or their corresponding edges. For the single (isolated)

dihedral, the scattering centre correctly identifies the apex of the dihedral with residual scattering centres not associated to the corresponding edges. These results were expected, given the sub-resolution cell dihedral dimensions and spacing of the dihedral pair.

2. ESPRIT with interpolation-based polar reformatting, correctly identifies the three primary scattering centres associated with the apex of each dihedral. However, it does not detect any edge diffraction components. From the ESPRIT resolution curves presented in Figure 6.1, an eigenvalue amplitude separation of approximately 100 dB is required to resolve a scatterer with an amplitude ratio of -25 dB and separation of ≈ 0.1 m. As shown in Figure 6.9, when using interpolation-based polar reformatting the separation achieved amounts to ≈ 100 dB, however, in this borderline case there is not sufficient difference between the noise components and the signal components to classify them as part of the signal subspace. In both FEKO and Matlab results, a slight bias in the measurements is observed as highlighted in Table 6.1.

3. ESPRIT with the iterative polar reformatting approach yields 11 scattering centre estimates positioned at:

   (a) The apex of each dihedral (3),

   (b) The edges of each dihedral (5),

   (c) A point behind the dihedral pair (equivalent to the apex of a larger dihedral projected from the boundary edges of the dihedral pair) (1),

   (d) A region behind the geometry (cross range of ≈ 0 m and slant range of ≈ -0.5 m) (2).

   The improved resolution and detection of the edges is a direct result of the improved eigenvalue separation between the signal and noise subspace, as shown in Figure 6.9. Given the known limitation of iterative polar reformatting under sub-resolution cell separation, this implementation makes use of the first 300 estimated scattering centres from EP-based CLEAN to seed a single iteration of the polar reformatting used with ESPRIT.

The two scattering centres identified behind the geometry align well with an observed peak structure in the ISAR overlay. It is assumed that this structure exists as a result of the scattering interaction between the edges of the joined dihedral pair and that of the third dihedral. In the same way, the existence of the scattering centre behind the joined dihedral pair is assumed to exist as a result of the scattering interaction between the edges of dihedral pair, effectively forming a large dihedral equivalent.

Conclusion

This investigation evaluated two scattering mechanisms (i.e. double bounce from the faces of the dihedrals and edge diffraction from the edges). When comparing the results from scattered field data generated in FEKO to that generated in Matlab, both the scattering centre estimates as well as the emerging algorithm characteristics (such as the eigenvalues from ESPRIT) are shown to be closely matched. This, in a way, has validated the assumption that certain scattering mechanism exhibit ideal point like scattering and that the techniques can perform well on more representative data. The results have also demonstrated an improvement in the performance of ESPRIT (in a more intuitive way) when using the iterative polar reformatting with EP-based CLEAN seeding.

7.1.4 Scatterer Trajectories and RCS Re-synthesis

Discussion of results

The results presented in Figures 6.11, 6.12 and 6.13 show the extracted scattering centres from overlapping 3 deg subsets of scattered field data. The data was generated in FEKO using the three dihedral geometry over a total scene rotation of 90 deg. A plot of the expected trajectories is shown as reference in Figure 6.10.

In each figure the three dominant scattering centres (highest amplitudes) are plotted in blue and the remaining ones in red. This is done in an attempt to

draw a distinction between the strong scattering expected at the apex of the three dihedrals and that from weaker scattering sources.

A summary of the observed trends follows:

EP-based CLEAN

From the trajectories presented in Figure 6.11:

1. A distinct persistent scattering centre is observed, the trajectory of which coincides with the apex of the isolated dihedral. There are a couple of scattering centres close to this trajectory, however, with no apparent correlation from scene to scene.
2. For the joined dihedral pair three distinct trajectories are observed with the following characteristics:
   (a) The centre trajectory forms in regions where a single strong peak (up to ≈ 3 dB larger than the return from the isolated dihedral) dominates. This corresponds to the amplitude trajectory with a sinusoidal pattern.
   (b) The two outer trajectories are shown to dominate in the absence of the strong centre peak.

   In regions where the single scattering centre dominates, residual trajectories are also formed the positions of which extend slightly past the outer two trajectories and appear merged in the results.

From the fact that the separation between each dihedral's apex, in the joined dihedral pair, is less than the functional resolution for EP-based CLEAN. It is then expected, given the phase dependency noted in Section 7.1.1, that when the geometry is rotated, the change in phase between the two primary scattering sources introduces an interference pattern that allows for regions where the two sources are resolved (two outer trajectories), and regions where they are not (centre trajectory).

ESPRIT

When using interpolation-based polar reformatting, see Figure 6.12, three

well defined trajectories are observed which coincide with the trajectories of each dihedral apex. The amplitudes from the primary trajectories appear more constant compared to EP-based CLEAN. This characteristic highlights the fact that ESPRIT better separates the underlying components, when compared to EP-based CLEAN whose amplitude estimates are directly affected by the interference.

Some additional trajectories are also shown, coinciding with the edge diffraction components, over the first and the last part of the total look angle. Over these regions a degradation in the accuracy of estimates is also observed. This is attributed to an expected partial correlation between the underlying spectral components, caused by imperfect polar reformatting and spatial smoothing.

When using iterative polar reformatting, see Figure 6.13, eight persistent and well defined trajectories are shown where the trajectories map well to those in the reference, see Figure 6.10. When compared to the interpolation-based polar reformatting results, the follow improvements are observed:

1. The amplitudes corresponding to the dominant scattering centres are more consistent with fewer outliers.
2. Edge diffraction components are observed over the centre region of the total look angle, however, they appear to be noisy.
3. Two additional broken-up trajectories appear behind the geometry.
4. A single additional, but noisy, trajectory is shown just behind the dihedral pair from -20 to 20 deg, most notably in the slant range vs aspect angle plot.

While the additional scattering components, which are the result of interaction between the three dihedrals, have already been discussed in Section 7.1.3. Figure 6.13 highlights that the lower amplitude scattering centres are less consistent, from scene to scene, with some amplitude modulation occurring. This is assumed to be the result of interference from other scat-

tering centers due to imperfect polar reformatting leading to a coupling of the spectral components as well as their amplitudes.

RCS Re-synthesis

The RCS calculated from the re-synthesised scattered field data, using the scattering centre estimates over the 90 deg look angle, is presented in Figure 6.14. The RCS mean as a function of aspect angle, where the mean was taken over frequency, demonstrates a lobing pattern similar to that observed in the amplitude trajectories in EP-based CLEAN. When compared to the RCS mean reported by FEKO, all three techniques appear to perform equally well. When comparing the RMSE, EP-based CLEAN and ESPRIT using interpolation-base polar reformatting appear to demonstrate similar performance, with errors ranging from -30 dB to around 5 dB. ESPRIT using iterative polar reformatting in shown to offer a significant improvement with errors ranging from -40 dB to around -15 dB.

Conclusion

The results from this investigation have shown that certain scattering mechanisms do in fact appear as localised radiation sources over significant angular sectors. While the amplitude and location may vary as a function of aspect angle, these scattering centres form well defined trajectories with clear relationships form scene-to-scene.

When the scattering centres are resolved with high accuracy, as shown for the ESPRIT estimates, the trajectories are deterministic from scene-to-scene. However, when the scattering centers are not resolved, as shown for the EP-based CLEAN estimates, the trajectories exhibit complex relationships from scene-to-scene. In both instances, the estimates are shown to produce high quality re-synthesised RCS with clear performance gains using the iterative polar reformatting technique. However, there are clear advantages to having deterministic trajectories such as: the ability to filter, track as well as model each scattering centre as a function of aspect angle.

7.2 Conclusions

In this study, two scattering centre extraction techniques, namely EP-based CLEAN and ESPRIT, have been evaluated. The objective was to ascertain their usefulness in establishing a preferred approach to scattering centre extraction in controlled environments. A direct comparison between ESPRIT and EP-based CLEAN has shown that ESPRIT offers improved performance in high SNR conditions, in terms of both resolution and measurement precision. The analysis was conducted on synthetic scattered field data generated by direct use of the ideal point scatterer model as well as using the computational electromagnetics methods available in FEKO. Given well matched results for both data sets, the use of the ideal point scatterer model to approximate localised scattering from certain objects has been validated.

The study has shown that at high SNR the achievable performance in the extension of ESPRIT to high resolution radar imagery is processing limited. This characteristic is shown to originate from the mapping of measurements made in polar space to Cartesian space followed by spatial smoothing. As a result of this limitation, a technique was developed which makes direct use of scattering centre estimates extracted with ESPRIT, to perform polar reformatting in a iterative manner. Some initial results have shown significant improvements in measurement precision with performance bounds limited only by the input SNR. A more robust implementation of the technique has also been proposed which makes use of EP-based CLEAN to provide the initial estimates to seed the algorithm, followed by the use of ESPRIT. This was proposed as a result of reduced performance gains when partially correlated scattering centres are present.

While ESPRIT has demonstrated superior performance when compared to EP-based CLEAN and as a result can be considered as the preferred approach to scattering centre extraction in controlled environments. The current extension of ESPRIT to high resolution radar imagery has certain performance limiting characteristics. It can therefore be concluded that the preferred approach includes the use of ESPRIT as well as supporting techniques which aim to mitigate the performance limiting characteristics. The proposed iterative polar reformatting

technique with EP-based CLEAN estimates used to initialise the algorithm can be classed as a supporting technique.

7.3 Future Work

From the insights gained during the study, the proposed future works aims to extend and improve the current development on a preferred approach to scattering centre extraction in controlled environments.

1. In this study, conventional interpolation-based polar reformatting methods were evaluated, such as nearest neighbour, bi-linear and cubic spline. More advanced techniques, such as bi-harmonic spline interpolation and equivalents can also be used and should be investigated in terms of their limitations as well as influence on the super-resolution techniques.

2. An analysis on the influence of polar reformatting on the underlying data model may help lead to an extension of the ESPRIT algorithm that maps directly to high resolution radar imagery.

3. Where the above deals with uniform-polar domain measurements non-uniform measurements in the polar space, which map directly to the uniform samples in Cartesian space can also be investigated.

4. The relationships between the expected performance as a function of inaccuracies on the model parameters (angle and frequency) should also be addressed. This evaluation will add value in extending super-resolution techniques outside of controlled environments.

Bibliography

[1] C. Özdemir, *Inverse Synthetic Aperture Radar Imaging with MATLAB Algorithms*. Hoboken, New Jersey: John Wiley and Sons, 2012.

[2] L. C. Potter and R. L. Moses, "Attributed Scattering Centers for SAR ATR," *IEEE Transactions on Image Processing*, vol. 6, pp. 79–91, January 1997.

[3] J. Tsao and B. D. Steinberg, "Reduction of sidelobe and speckle artifacts in micorwaveimaging: The CLEAN technique," *IEEE Transactions on Antennas and Propagation*, vol. 36, pp. 543–556, April 1988.

[4] S. Yiping and L. Pingping, "An Improved Method of ISAR Image Formation," *Proc. 35th Midwest Symp. Circuits and Syst*, vol. 2, pp. 983–986, August 1992.

[5] R. Bose, A. Freedman, and B. Steinberg, "Sequence CLEAN: a modified deconvolution technique for microwave images of contiguous targets," *IEEE Transactions on Aerospace and Electronic Systems*, vol. 38, pp. 89–97, January 2002.

[6] R. Bose, "Sequence CLEAN technique using BGA for contiguous radar target images with high sidelobes," *IEEE Transactions on Aerospace and Electronic Systems*, vol. 39, pp. 368 – 373, January 2003.

[7] I. S. Choi and H. T. Kim, "Two-dimensional evolutionary programming-based CLEAN," *IEEE Transactions on Aerospace and Electronic Systems*, vol. 39, pp. 373 – 382, January 2003.

[8] W. Yang, C. Jianwen, and L. Zhong, "Research on radar imaging of manoeuvering targets," in *Proceedings of the International Radar Conference*, pp. 42 – 44, September 2003.

[9] M. Martorella, N. Acito, and F. Berizzi, "Statistical CLEAN Technique for ISAR Imaging," *IEEE Transactions on Geoscience and Remote Sensing*, vol. 45, pp. 3552–3560, November 2007.

[10] V. F. Pisarenko, "The retrieval of harmonics from a covariance function," *Geophys. J. Roy. Astron. Soc.*, vol. 33, pp. 247–266, 1973.

[11] R. Schmidt, "Multiple Emitter Location and Signal Parameter Estimation," *IEEE Transactions on Antennas and Propagation*, vol. 34, pp. 276 – 280, March 1986.

[12] R. Roy, T. Kailath, and A. Paulraj, "Direction-of-arrival estimation by subspace rotation methods - ESPRIT," in *IEEE International Conference on Acoustics, Speech, and Signal Processing, ICASSP-86*, vol. 11, pp. 2495 – 2498, April 1986.

[13] M. Wax and T. Kailath, "Detection of signals by information theoretic criteria," *IEEE Transactions on Acoustics, Speech and Signal Processing*, vol. 33, pp. 387 – 392, April 1985.

[14] T.-J. Shan, M. Wax, and T. Kailath, "On Spatial Smoothing for Direction-of-Arrival Estimation of Coherent Signals," *IEEE Transactions on Acoustics, Speech and Signal Processing*, vol. 33, pp. 806 – 811, August 1985.

[15] R. Roy and T. Kailath, "ESPRIT-Estimation of Signal Parameters Via Rotational Invariance Techniques," *IEEE Transactions on Acoustics, Speech and Signal Processing*, vol. 37, pp. 984 – 995, July 1989.

[16] J. W. Odendaal, E. Barnard, and C. W. I. Pistorius, "Two-dimensional superresolution radar imaging using the MUSIC algorithm," *IEEE Transactions on Antennas and Propagation*, vol. 42, pp. 1386 – 1391, October 1994.

[17] C.-C. Yeh, J.-H. Lee, , and Y.-M. Chen, "Estimating two-dimensional angles of arrival in coherent source environment," in *International Conference on Acoustics, Speech, and Signal Processing, ICASSP-88*, vol. 5, (New York), pp. 2909 – 2912, April 1988.

[18] Y.-M. Chen, "On Spatial Smoothing for Two-Dimensional Direction-of-Arrival Estimation of Coherent Signals," *IEEE Transactions on Signal Processing*, vol. 45, pp. 1689 – 1696, July 1997.

[19] O. Dobre and E. Radoi, "Advances in subspace eigenanalysis based algorithms: from 1D toward 3D superresolution techniques," in *5th International Conference on Telecommunications in Modern Satellite, Cable and Broadcasting Service, TELSIKS 2001*, vol. 2, pp. 547 – 554, September 2001.

[20] E. Radoi, A. Quinquis, and F. Totir, "Achieving superresolution by subspace eigenanalysis in multidimensional spaces," in *Proc. EUSIPCO 2002 Conf.,*, (Toulouse, France), 2002.

[21] Y. Hua, "Estimating two-dimensional frequencies by matrix enhancement and matrix pencil," *IEEE Transactions on Signal Processing*, vol. 40, pp. 2267 – 2280, September 1992.

[22] X. Gu, Y. Zhang, and X. Zhang, "Electromagnetic simulation of ISAR imaging with supper-resolution," in *1st Asian-Pacific Conference on Synthetic Aperture Radar, APSAR 2007*, (Huangshan, China), 2007.

[23] X. Gu and Y. Zhang, "Effects of amplitude and phase errors on 2-D MUSIC and 2-D ESPRIT algorithms in ISAR imaging," in *2nd Asian-Pacific Conference on Synthetic Aperture Radar, APSAR 2009*, (Xian, Shanxi, China), 2009.

[24] A. Quinquis, E. Radoi, and F.-C. Totir, "Some Radar Imagery Results Using Superresolution Techniques," *IEEE Transactions on Antennas and Propagation*, vol. 52, pp. 1230–1244, May 2004.

[25] M. L. Burrows, "Two-Dimensional ESPRIT with Tracking for Radar Imaging and Feature Extraction," *IEEE Transactions on Antennas and Propagation*, vol. 50, pp. 524–532, February 2004.

[26] D. G. Manolakis, V. K. Ingle, and S. M. Kogon, *Statistical and adaptive signal processing*. London: Artech House, 2005.

[27] A. W. Rihaczek and S. J. Hershkowitz, *Radar Resolution and Complex-Image Analysis*. London: Artech House, 1996.

[28] M. A. Richards, J. A. Scheer, and W. A. Holm, *Principles of Modern Radar, Basic Principles*. Chelsea, MI: Scitech, 2010.

EBE Faculty: Assessment of Ethics in Research Projects

Any person planning to undertake research in the Faculty of Engineering and the Built Environment at the University of Cape Town is required to complete this form before collecting or analysing data. When completed it should be submitted to the supervisor (where applicable) and from there to the Head of Department. If any of the questions below have been answered YES, and the applicant is NOT a fourth year student, the Head should forward this form for approval by the Faculty EIR committee: submit to Ms Zulpha Geyer (Zulpha.Geyer@uct.ac.za; Chem Eng Building, Ph 021 650 4791). Students must include a copy of the completed form with the thesis when it is submitted for examination.

Name of Student:	**Richard van Schalkwyk**
Department:	**Electrical Engineering**
Degree:	**M.Eng (Radar and Electronic Defence)**
Supervisors:	**Prof. Michael Inggs (UCT)** **Johan Smit (CSIR)**
Sponsorship:	**CSIR and ARMSCOR**
Research Project Title:	**Scattering Centre Extraction in High Resolution Radar Imaging**

Overview of ethics issues in your research project:.

Question 1: Is there a possibility that your research could cause harm to a third party (i.e. a person not involved in your project)?	YES	NO
Question 2: Is your research making use of human subjects as sources of data? If your answer is YES, please complete Addendum 2.	YES	NO
Question 3: Does your research involve the participation of or provision of services to communities? If your answer is YES, please complete Addendum 3.	YES	NO
Question 4: If your research is sponsored, is there any potential for conflicts of interest? If your answer is YES, please complete Addendum 4.	YES	NO

If you have answered YES to any of the above questions, please append a copy of your research proposal, as well as any interview schedules or questionnaires (Addendum 1) and please complete further addenda as appropriate.

I hereby undertake to carry out my research in such a way that

- there is no apparent legal objection to the nature or the method of research; and
- the research will not compromise staff or students or the other responsibilities of the University;
- the stated objective will be achieved, and the findings will have a high degree of validity;
- limitations and alternative interpretations will be considered;
- the findings could be subject to peer review and publicly available; and
- I will comply with the conventions of copyright and avoid any practice that would constitute plagiarism.

Signed by	**Full name & Signature**	**Date**
Student		

This application is approved by:

Supervisor (if applicable):		
HOD (or delegated nominee): Final authority for all assessments with NO to all questions and for all undergraduate research.		
Chair : Faculty EIR Committee For applicants other than undergraduate students who have answered YES to any of the above questions.		